POLITECNICO DI TORINO

Master's Degree in Aerospace Engineering

Master's Degree Thesis

Design of Guidance and Algorithms for Space Rendezvous Maneuvers

Supervisors

Prof. ELISA CAPELLO

Prof. HYEONGJUN PARK

Candidate

SIMONE DASCANIO

2021

Summary

CubeSat technology has been widely studied in the last 20 years, especially for missions in Low-Earth-Orbit (LEO). It represents an interesting alternative to multisatellite missions with bigger spacecrafts thanks to their superior agility and low cost. When these nanosatellites are operating to achieve a docking mission, it is essential to carefully plan rendezvous maneuvers and proximity operations to ensure mission safety and success. The aim of this research is to design and evaluate the performance of guidance and control algorithms for orbital rendezvous maneuvers. Zero-Effort-Mission/Zero-Effort-Velocity (ZEM-ZEV) guidance and Linear Quadratic Regulator (LQR) control are investigated to achieve position and attitude control for two 3U CubeSats in different scenarios.

The first mission scenario considers the chaser in an initial station keeping point behind the target on a lower orbit. The approach trajectory starts with a homing phase to rise the chaser altitude and get to the target orbit, then a closing phase decreases the distance with the target until a final station keeping point is reached. A ZEM-ZEV guidance is implemented to control the chaser position during the target approach. This guidance, commonly applied to asteroids intercept and landing, is an optimum law only if the target gravitational field is a function of time. Moreover, this algorithm has a good accuracy, low fuel consumption, and effectiveness in presence of external disturbances. The ZEM-ZEV guidance is modified to adapt it to the rendezvous problem. In order to ensure that the chaser actually follows the defined trajectory, the actual position and velocity of the spacecraft are compared with the ideal ones at each time step. This method also allows low control accelerations.

The second scenario is a short range maneuver. As before a homing phase followed by the closing phase is executed to reach a final station keeping point few meters behind the target. The objective of this mission is to test the precision of the Guidance, Navigation and Control (GNC) system during proximity operations before a docking. Therefor, a collision avoidance maneuver is also implemented where the chaser moves away from the target along a semicircular trajectory. An

LQR law is proposed to control the chaser position along the maneuver. The LQR feedback gain is computed from the Hill equations of the relative motion and the cost weighting matrices are chosen from a trade-off in order to balance the requirements of following the desired trajectory and minimize the fuel consumption.

An attitude control system is finally studied for the chaser to ensure the possibility to hold or modify the orientation throughout the maneuver, acting against the external torques. Euler's equations are formulated for the dynamics while the kinematics is based on quaternions to avoid rotational sequences and singularities at any attitude. The feedback control exploits an LQR method based on the linearized dynamics equations.
The work is completed with a proposed combination of attitude control and position control for the second scenario.

Keywords: space, satellite, cubesat, rendezvous, proximity operations, Zero-Effort-Mission/Zero-Effort-Velocity, guidance, LQR.

Acknowledgements

My sincere gratitude goes to Dr. Elisa Capello from Politecnico di Torino and Dr. Hyeongjun Park from New Mexico State University for their precious help during my thesis.
I would like to sincerely thank my family for all the support they gave me through all these years. This is the end of a long journey that I could only achieve thanks to their support. A warm thought also goes to my dear and old friends: Giulio, Ivan, Gabriele. Your friendship gave me strength even in the darkest moments.

Table of Contents

List of Tables

List of Figures

Acronyms

LEO
Low-Earth-Orbit

ZEM-ZEV
Zero-Effort-Miss/Zero-Effort-Velocity

LQR
Linear Quadratic Regulator

LQI
Linear Quadratic Integral

RVD
Rendezvous and Docking

LM
Lunar Module

CSM
Command/Service Module

SSO
Space Shuttle Orbiter

ISS
International Space Station

LOS
Line of Sight

Chapter 1

Introduction

1.1 Literature Review & Motivation

1.1.1 Rendezvous

With the terms of rendezvous and docking we refer to a typical maneuver in space between two vehicles, in order to approach each other and join together. Since the 1960s, a lot of work have been done on how to accomplish a rendezvous and docking maneuver, both manually and autonomously between spacecraft. It is fair to say that most of the work and experiences in manual and automated rendezvous and docking come from NASA and Russian space programs. Historically, U.S. followed a manual approach to rendezvous and docking, in opposition to Russia which aimed at developing automated and standardized maneuvers. The first successful attempt in executing a rendezvous and docking came with the Gemini program in 1960's, where the spacecraft was required to dock with a second stage booster on a circular orbit [1]. This was the first step toward the Apollo program and a rendezvous maneuver was finally accomplished between the lunar module (LM) coming up from the sea of Tranquility and the command/service module (CSM) on a near circular orbit around the Moon in 1969. The LM, after the phasing, reached a position around 50 km behind the target on a lower orbit and from here the thrusters were fired with an elevation angle of $\phi = 26.5°$ to bring the spacecraft on a transfer orbit and approach few meters in front of the CSM [2].

Later the Space Shuttle Orbiter (SSO) was developed with the objective of carrying space systems in the space and performed maintenance. It was able to dock with the Mir station and lately with the International Space Station (ISS). Unlike its predecessors, the Space Shuttle was able to execute an autonomous rendezvous, except for the last meters before the docking where the man in the loop was needed [3]. After the SSO, many fully autonomous vehicles have been developed to bring resources on board the ISS, such as ATV [4], HTV [5], Progress

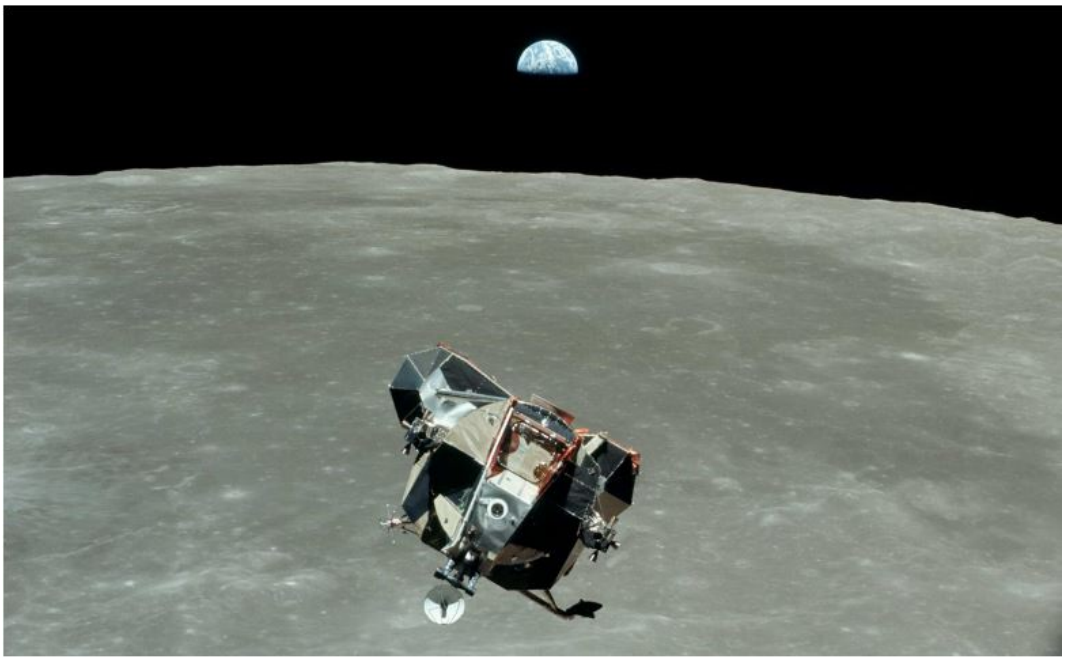

Figure 1.1: Apollo 11 rendezvous seen from the CSM [2].

[6] and Cygnus [7].

Commonly, a rendezvous and docking maneuver is formed of four main parts: phasing, far range rendezvous, close range rendezvous, and final approach [3]. The launcher places the spacecraft on an orbit but due to positioning errors is not able to reach exactly the target orbit in Low-Earth-orbit (LEO) cases. The chaser is usually brought on an orbit few kilometers below the target one. The first maneuver is then the phasing where the spacecraft operates to correct eventual imprecisions in the orbital parameters such as Right Ascension of the Ascending Node (RAAN) and inclination and to reduce the distance of the chaser from the target. The HTV, ATV, and SSO, for example, follow similar phase adjustments. They start on a lower orbit maneuvering and they gradually increase the apogee and perigee in order to get closer to the final orbit. Except the SSO which reaches directly the target orbit, they stop on a lower orbit with respect to the target and still far behind it. Here the free drift toward the target, due to their lower position, is used to get closer to the target without fuel consumption [3],[4],[5].

After the phasing, the far range rendezvous starts. This phase, also known as homing, is usually dedicated to bring the chaser on the target orbit, reducing its velocity and the distance from the target. The homing also defines the point

where the spacecraft switches from absolute to relative navigation measurement of positions and velocities [3]. Vehicles as the ATV and HTV follow a Hohmann maneuver to save propellant, while the SSO applies a radial boost and moves along a semicircular trajectory [3],[4],[5]. If the target presents a safety volume around it, as for the ISS, then a constraint is imposed to the position of the final station keeping point reached during the homing.

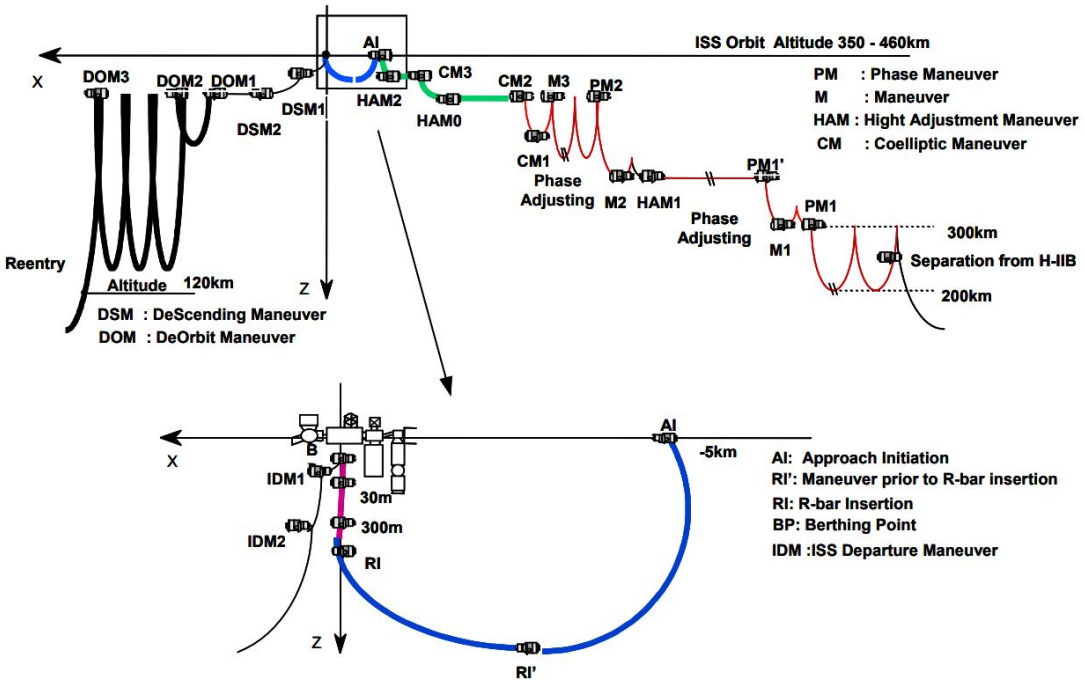

Figure 1.2: HTV rendezvous, docking and reentry [5].

The next step is the close range rendezvous which allows to get from the last station-keeping point in to the close proximity behind the target. Many are the implementable trajectories as shown in Fig. 1.3. It is possible to get closer to the target staying on the target orbit and sliding toward it from in front or behind the target. Another strategy is to move below the target with a fly around maneuver from the target orbit. Starting the fly around from the target orbit, the safety factor is increased since the spacecraft starts from a station-keeping point with a constant distance from the target, but it is also possible to reach below the target directly from a lower orbit, where the timing is going to be essential. The SSO moves on a semicircular trajectory and from behind it gets few meters in front of the ISS or in other occasions it executes a fly around and arrives under the target, depending on the docking port position [3]. The HTV and ATV follow very similar trajectories: they fire the thrusters in a radial direction

and move along a semicircular maneuver until they are close behind the target [3],[4].

The last maneuver is the final approach and it is used to get the spacecraft to the docking port. It is commonly a straight-line trajectory starting from the last close range position. This kind of approach is implemented for the last 300 m of both the HTV and ATV. The SSO follows a similar maneuver but it is executed manually by the crew pilot.

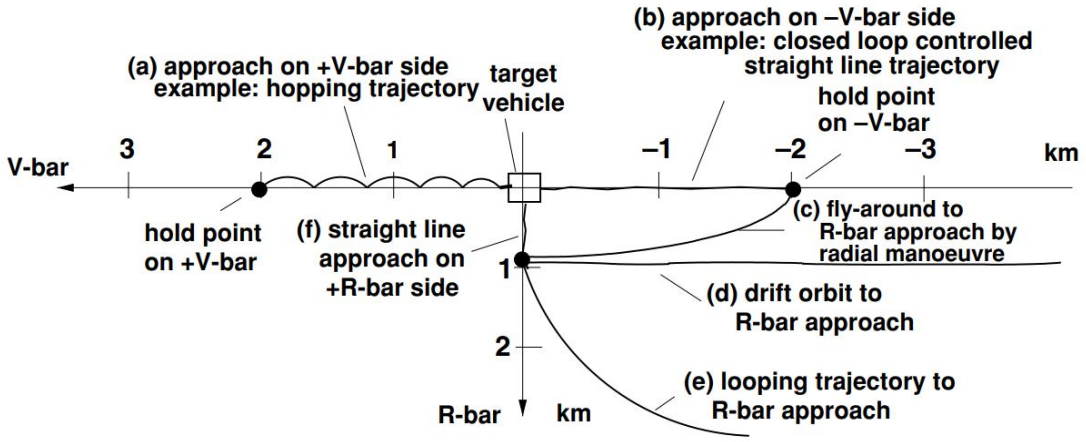

Figure 1.3: V-bar/R-bar approach for the close range [3].

Today, the objective would be to obtain the same results with small satellites such as CubeSats. Due to their small dimensions, it is a challenging task: most of the space technologies (thrusters, reaction wheels and electronics) must be miniaturized to be mounted on small satellites so that it is hard to reach the same level of accuracy. For these reasons, rendezvous and docking maneuver is a topic of high interest still today. In fact, this technology could lead to many interesting applications, such as launching a constellation of CubeSats operating in close proximity (formation flying) or to accomplish space assembling. The research developed in [8] and sponsored by ESA can be considered one of the few comprehensive works on this topic. The objective is to develop a rendezvous maneuver between two 6U CubeSats starting from the far range approach and following a similar trajectory to the ones seen before for autonomous vehicles, such as ATV and HTV. The maneuver ends with a full hard docking between chaser and target.

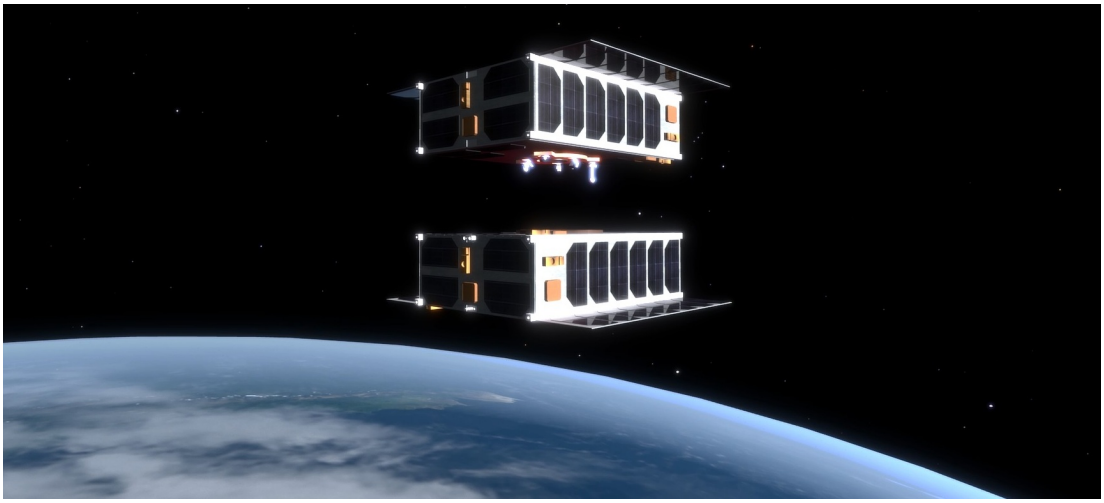

Figure 1.4: Illustration of the final approach between two 6U CubeSats [8].

1.1.2 Guidance

A guidance function in general has the aim to bring a spacecraft from an initial angular or linear position and velocity to a final position and velocity acting against external disturbances. The guidance must be able to minimize the fuel consumption or the time of flight, depending on the flight purpose. Based on the chaser's relative position and velocity with respect to the target, the guidance will compute the accelerations necessary to follow the trajectory and achieve the final conditions, and the time left to accomplish the maneuver. As specified in [9], guidance laws can be split in two different categories: predictive guidance and feedback guidance. The last type is known to be robust against uncertainties, with low computational cost, safe and it can be implemented to follow a desired trajectory. For all these reasons, a feedback law is of interest in this study.

Most of the guidance laws developed in literature are for the problem of moving a chaser in the proximity of a specified target. In many researches, such as in [9],[10], a proportional navigation (PN) guidance is chosen for the rendezvous and dock problem. The PN guidance computes the accelerations needed to reach the target and controls the component of relative velocity normal to the line of sight (LOS) at each instant. As explained in [11], this guidance method is mainly used for missile interceptions so when applied to rendezvous and docking it must be consider to not only drive to zero the component of relative velocity perpendicular to LOS but also the one along the LOS, to guarantee that the chaser stops when reaches the target. The concept of zero-effort-velocity (ZEV) error, which defines the difference between the target and chaser velocity is introduced in [12]. It is analog to the concept of

zero-effort-miss (ZEM) distance, which can be often found in the expression of the PN guidance acceleration commands [10]. A zero-effort-miss/zero-effort-velocity (ZEM-ZEV) guidance law was then derived in [10], where it is shown how this algorithm is an optimum feedback guidance only if the gravitational field can be considered constant or if at least it is only a function of time. As it is described in [13],[14], the ZEM-ZEV approach has mainly been studied for asteroids interception and proximity operations or for planetary landing. The ZEM-ZEV algorithm computes the accelerations required to reach the final position and velocity, as well as guarantees to optimize the fuel consumption (minimizing the required ΔV). As described in [9],[15], the main problem in applying this approach for a rendezvous and docking is that it is not possible to follow the desired maneuver. In fact, a completely different trajectory is generated if the accelerations are computed only based on the offset in position and velocity between the target and the chaser. In this research, a modified ZEM-ZEV guidance is implemented and its performance is evaluated for the long-range maneuver. The major advantages of this algorithm are the increased precision in following a specified trajectory, especially if it has a significant curvature, as well as a reduction in fuel consumption.

1.1.3 Control

The control function has the objective to guarantee that the spacecraft follows the required trajectory and achieves the desired attitude. To accomplish this task, the control law produces a control force or torque as output which is then sent to the actuators. Here a position and attitude control are implemented for a mission of docking and rendezvous of two CubeSats.

In literature, it is possible to find a wide variety of control laws for rendezvous operations. They are typically classified in two categories: non-linear and linear control theories. Here only the second class is considered, in fact non-linear controls can work correctly even for far-range rendezvous without introducing errors on the actual position and velocity, but they introduce heavy computational effort. The Clohessy-Wiltshire-Hill equations of the relative motion are here developed for the problem. It is a linear model frequently used to describe the relative motion of a chaser on a circular orbit. In [8], a linear quadratic integral (LQI), a robust H_∞, and a linear quadratic regulator (LQR) are developed for the position control of a far and close range rendezvous. The H_∞ seems to be the most robust control among the ones analysed while the LQR lack in precision. Also, in [16], an LQR control is tested for a rendezvous. It is observed from the results that the control is sub-optimum, in fact a significant control action is required to reach the final position and velocity with a consequent augmented ΔV. The final waypoints are reached with low accuracy and the shape of the trajectories is quite different from

the desired one. It is interesting to notice that it is possible to highly increase the LQR performance if the gain matrix is computed with the weighting matrices varying in time as in [17].
Unlike the Hill equations, the Euler's equations for attitude dynamics are non-linear, so in order to apply an LQR control they need to be linarized. In [18], it is shown how the LQR can provide a good trade-off between time response and energy, with an adequate tuning of the weighting matrices.

The LQR control is not in general a robust control but it is simple and easy to tune. Additionally, it also allows to find a compromise between accuracy and maneuver cost through the weighting matrices. Hence, in this research, an LQR law is developed for both position and attitude control, and then their performance is evaluated.

1.2 Overview of the Thesis

The objective of this research is to study the problem of autonomous rendezvous and docking (RVD) between CubeSats. Two different scenarios are considered where two 3U CubeSats are positioned far away from each other in a low Earth orbit. It is defined at first a long-range maneuver with the chaser and target distant with few kilometers from each other. A ZEM-ZEV guidance is chosen and implemented for this mission because of its low computational effort and low fuel consumption. The ZEM-ZEV guidance is initially developed to enable spacecraft precision landing on asteroids or planets, here we try to evaluate the performance of this closed-loop guidance applied to the RVD problem.

In the second part of the work, a close-range maneuver is developed. The chaser is able to arrive within few meters from the target and then an abort mission maneuver is considered to distance the chaser again and avoid a possible collision with the target. An LQR controller is used for the position control of the chaser along the maneuver. The choice is justified considering that LQR is widely used for spacecrafts GNC and many examples are in literature. The attitude is controlled with three miniaturized reaction wheels, one for each body axis. Again, an LQR control is considered for it. Once the LQR position and attitude controllers are developed, they are combined together to build the complete attitude and orbit control system (AOCS).

This thesis is organised as follows:
Chapter 2 provides a description of the reference frames considered and of the transformation matrices to pass from one frame to another. Then the relative

motion equations, the attitude dynamic and kinematic equations are presented. The trajectories implemented during the approach are also explained. Chapter 3 describes the methodology of the ZEM-ZEV guidance and the LQR control theory. Chapter 4 presents the results obtained from the simulation of the case studied. Finally, Chapter 5 provides the conclusions and future work.

Chapter 2

Mathematical model

In the first part of this chapter, all the mathematical instruments needed to develop the rendezvous maneuver and the proximity operations are described. The coordinate systems used are briefly defined, and so are also the Clohessy-Wiltshire equations for the relative motion between the chaser and the target. The dynamics and kinematics equations for the attitude of the chaser are also described in their quaternion formulation.
In the second part of the chapter, the phases of a rendezvous maneuver are explained. Also, for each of them the ideal ΔVs and accelerations are computed. The mathematical formulation of the most relevant external disturbances for a low-Earth-orbit spacecraft is then presented.

2.1 Reference Frames

Three main reference frames are needed to fully describe the attitude and the relative motion of a spacecraft around the Earth:

- Earth-Centered Inertial Frame
- Orbital Frame
- Body Frame

These are the ones needed to build the orbit simulation.

2.1.1 Earth-Centered Inertial (ECI) Frame

The system, F_{IJK} originates at the Earth center of mass. Out of simplicity the Earth is usually defined as a sphere with an homogeneous distribution of mass so the origin of the frame coincides with the Earth geometric center. This frame is

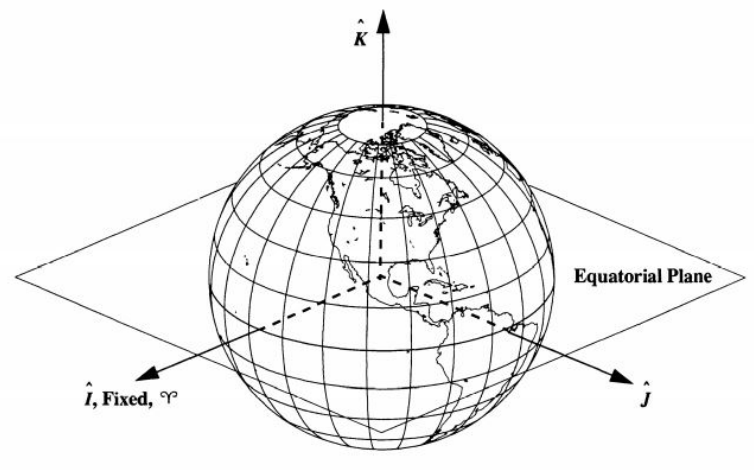

Figure 2.1: Geocentric Equatorial System, IJK [19].

also often referred to as IJK. The $\hat{I}$ axis points toward the capricornus constellation. This orientation is defined as the direction pointing from the center of the Earth to the center of the Sun when the Earth passes for the vernal equinox. The $\hat{J}$ axis lays in the equatorial plane, as shown in Figure 2.1, with the $\hat{I}$ axis. The $\hat{K}$ axis instead completes the right-handed coordinates, being perpendicular to the equatorial plane and pointing in the hemisphere where the North Pole is found. This system is considered to be fixed in space and it is commonly used to describe the motion of satellites around the Earth. In reality, the Earth is also moving which means that the ECI is not actually inertial, but it can be considered as if it was for small objects in orbit around it.

2.1.2 Orbital Frame

Also called the Local-Vertical/Local-Horizontal, F_{LVLH}, the orbital frame is widely used to describe the relative motion of a spacecraft, named chaser, with respect to a second satellite, the target, which is also moving around the Earth. The system is fixed in the target center of mass, O_{LVLH}. The spacecraft are treated as point masses, not as 3D bodies. The $\hat{z}_{LVLH}$ axis is here considered directed toward the Earth but there is not a fixed convention, so in literature it can be found with opposite verse. The $\hat{x}_{LVLH}$ is parallel to the spacecraft component of velocity tangent to the local orbit track and it is always perpendicular to $\hat{z}_{LVLH}$. Both $\hat{x}_{LVLH}$ and $\hat{z}_{LVLH}$ lay on the target orbit plane. Finally, the $\hat{y}_{LVLH}$ is found consequently by the right-handed rule and it is directed out of the orbit plane.

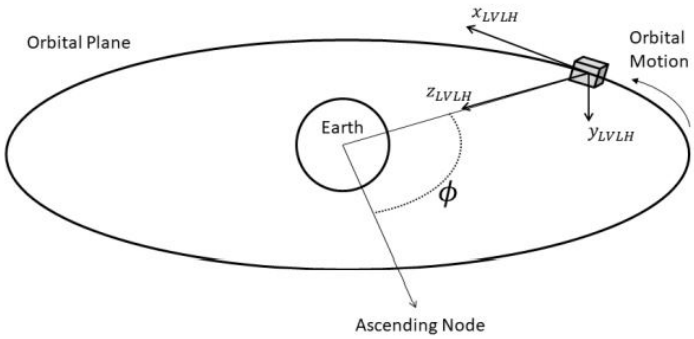

Figure 2.2: Orbital frame [16].

2.1.3 Body Frame

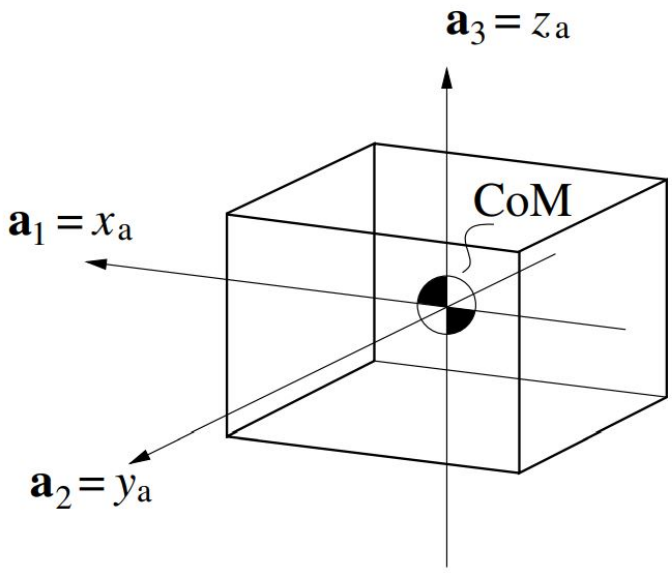

Figure 2.3: Body frame [3].

The body frame, F_B is typically used to describe the absolute attitude of a spacecraft and the rotations around its center of mass. This frame is fixed in the center of mass, O_B. It is worthy to mention that in general the center of mass of a spacecraft changes during the mission: the main reason is the lost propellant during the maneuver which causes a mass reduction. Other secondary reasons are also the propellant slosh, solar panel deployment or the release of a tether for gravity-gradient stabilization. Here out of simplicity, we do not consider this effect.

The directions of the body frame axes are not in general uniquely defined. It is thou quite common to consider $\hat{x}_B$ aligned with the docking axis direction at the end of the rendezvous, which in this case is the same as the $\hat{x}_{LVLH}$. The other two axes $\hat{y}_B$ and $\hat{z}_B$ are on the same plane perpendicular to the $\hat{x}_B$ unit vector. This coordinate system is also completely free to move with respect to the orbital frame.

2.1.4 Transformation Matrices

In the paragraph before, the coordinate frames of interest have been described. It is useful in many occasion to express the motion of a body or its attitude in a different reference frame from the one which has been defined in to. For this reason transformation matrices are used to pass from one reference frame to another. Here, the coordinate transformation from the orbital frame to the body frame is considered. It is important to notify that the combination of Euler's angles, ϕ, θ, ψ which is possible to use to build the rotation matrices and move from one frame to others are numerous, while the orientation between the two considered frames is uniquely defined. Here, a yaw-pitch-roll or 3-2-1 sequence has been considered. The order of the rotations sequence is important because rotations do not commute. The resulting matrix rotation is then,

$$L_{BLVLH} = \begin{bmatrix} 1 & 0 & 0 \\ 0 & \cos\phi & \sin\phi \\ 0 & -\sin\phi & \cos\phi \end{bmatrix} \begin{bmatrix} -\sin\theta & 0 & \cos\theta \\ 0 & 1 & 0 \\ \cos\theta & 0 & \sin\theta \end{bmatrix} ... \\ ... \begin{bmatrix} \cos\psi & \sin\psi & 0 \\ -\sin\psi & \cos\psi & 0 \\ 0 & 0 & 1 \end{bmatrix} \tag{2.1}$$

so the reference transformation will have the following expression,

$$\begin{bmatrix} x_B \\ y_B \\ z_B \end{bmatrix} = \begin{bmatrix} 1 & 0 & 0 \\ 0 & \cos\phi & \sin\phi \\ 0 & -\sin\phi & \cos\phi \end{bmatrix} \begin{bmatrix} -\sin\theta & 0 & \cos\theta \\ 0 & 1 & 0 \\ \cos\theta & 0 & \sin\theta \end{bmatrix} ... \\ ... \begin{bmatrix} \cos\psi & \sin\psi & 0 \\ -\sin\psi & \cos\psi & 0 \\ 0 & 0 & 1 \end{bmatrix} \begin{bmatrix} x_{LVLH} \\ y_{LVLH} \\ z_{LVLH} \end{bmatrix} \tag{2.2}$$

As illustrated in Figure 2.4, a first rotation of ψ is accomplished around the z-axis and an intermediate reference frame, F', is reached. A rotation of θ follows now around the y'-axis, so to get to F". From here the last rotation of ϕ is executed around x"-axis allowing to finally reach the desired orientation.

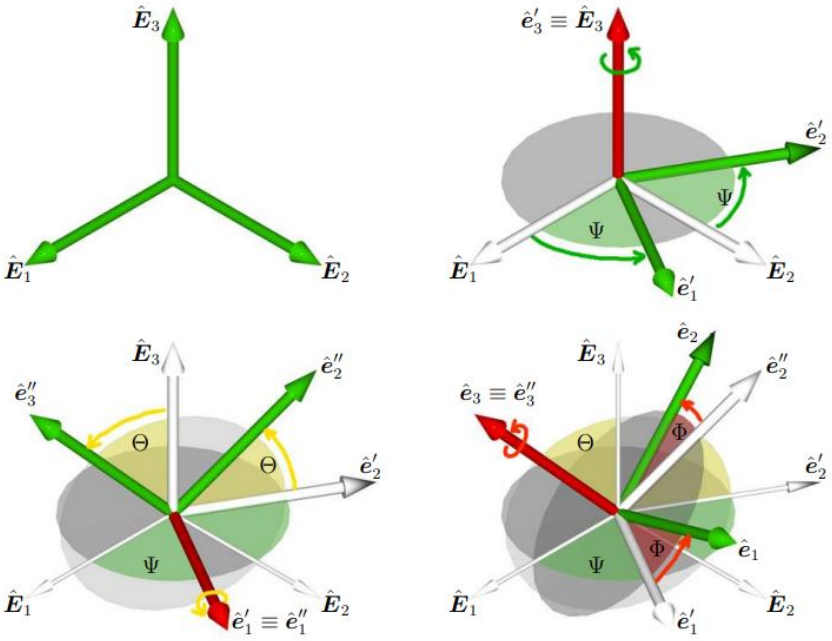

Figure 2.4: Euler's angles or 3-2-1 rotation [20].

2.2 Relative Motion Dynamics

To study the problem of rendezvous and proximity operations, a set of equations is derived to describe the motion of a chaser with respect to a target object. Many are the relative motions modeled which can be found in literature: one example is the Tschauner-Hempel (TH) equations which are used to describe the relative motion on an elliptical orbit [21]. Here out of simplicity the Hill equations are considered. They are applicable under two main conditions: the distance between the chaser and the target must be small compared to the distance between the target and the center of mass of the attracting planet and the considered orbit is circular or near-circular. To derive the Hill equations, a spacecraft is imagined immerse in a spherical gravitational field and acting on it are the forces due to external disturbances and from the thrusters. It is possible to write the Newton's law of gravitation as,

$$\bar{F}_g(r) = -GM\frac{m}{r^2}\frac{\bar{r}}{r} = -\mu\frac{m}{r^3}\bar{r} \tag{2.3}$$

where $\bar{r}$ is the position vector of the object in an inertial fame, G is gravitation universal constant, M is the Earth mass and m is the object's mass under the Earth's gravitational force. Hence, using this equation the accelerations acting on

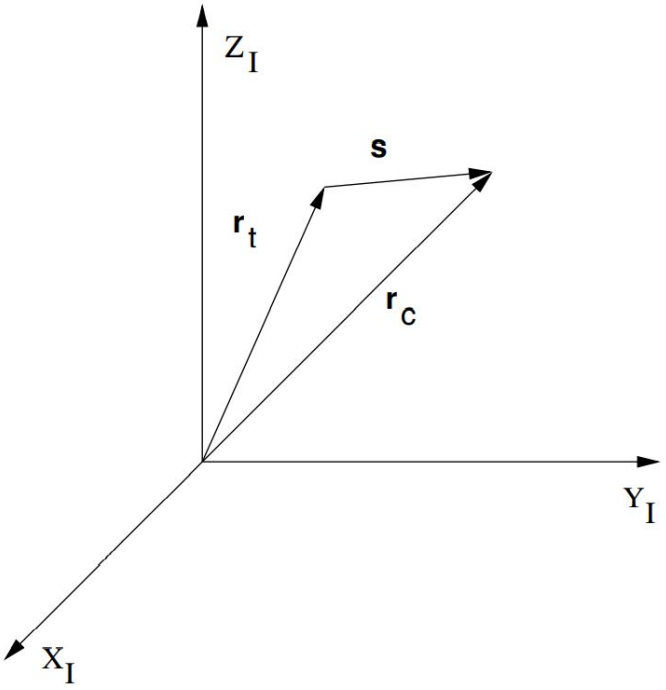

Figure 2.5: Target, r_t, and chaser, r_c, position in ECI frame [3].

the chaser and target are computed,

$$\ddot{\bar{r}}_c = \frac{\bar{F}_g}{m_c} + \frac{\bar{F}}{m_c} = -\frac{\mu}{r_c^3}\bar{r} + \frac{\bar{F}}{m_c} \tag{2.4}$$

$$\ddot{\bar{r}}_t = \frac{\bar{F}_g}{m_t} = -\frac{\mu}{r_t^3}\bar{r} \tag{2.5}$$

for the target is imagined that only the gravitational force is present, while for the chaser the effect of other forces, such as external disturbances and actuation, are considered. At this point, the relative position between target and chaser can be expressed as

$$\bar{s} = \bar{r}_c - \bar{r}_t \tag{2.6}$$

where the vector $\bar{s}$ is now differentiated two times to find the accelerations and then the component of the gravitational force per unit mass, $f_g(\bar{r})$, is linearised for small values of $\bar{r}_t$ (for a full discussion see reference [3]). As a result a new expression of $\ddot{\bar{s}}$ is obtained and it is then transformed in a relative reference frame

with origin fixed on the target

$$\ddot{\bar{s}}^* + \bar{\omega} \times (\bar{\omega} \times \bar{s}^*) + 2\bar{\omega} \times \dot{\bar{s}}^* + \dot{\omega} \times s^* + \frac{\mu}{r_t^3} M\bar{s} = \frac{\bar{F}}{m_c} \tag{2.7}$$

where s^* is the distance between target and chaser expressed in the relative frame and ω is the target angular velocity. Finally, it can be found the system of equations describing the relative motion, the Hill's equations

$$\begin{aligned} \ddot{x} - 2\omega\dot{z} &= \frac{F_x}{m_c} \\ \ddot{y} + \omega^2 y &= \frac{F_y}{m_c} \\ \ddot{z} + 2\omega\dot{x} - 3\omega^2 z &= \frac{F_z}{m_c} \end{aligned} \tag{2.8}$$

In Equation 2.8, $\omega = \frac{2\pi}{T}$ represents the angular velocity of the target orbit and m_c is the chaser mass. The relative motion can be influenced by the accelerations $\gamma_{x,y,z} = \frac{F_{x,y,z}}{m_c}$ which are the sum of the external disturbances acting on the chaser and the applied thrust. $\ddot{x}$, $\ddot{y}$ and, $\ddot{z}$ represent the relative accelerations. This solution does not take in count the orbit curvature so the results have an error which grows with the distance from the target coordinate system. For this study, the CW equations are considered later for the ZEM-ZEV guidance and the LQR control. The resulting integrated equations are:

$$\begin{aligned} x(t) = &(\frac{4\dot{x}_0}{\omega} - 6z_0)\sin\omega t - \frac{2\dot{z}_0}{\omega}\cos\omega t + (6\omega z_0 - 3\dot{x}_0)t + (x_0 + 2\frac{z_0}{\omega}) + ... \\ &+ \frac{2}{\omega^2}\gamma_z(\omega t - \sin\omega t) + \gamma_x(\frac{4}{\omega^2}(1 - \cos\omega t) - \frac{3}{2}t^2) \end{aligned} \tag{2.9}$$

$$y(t) = y_0\cos\omega t + \frac{\dot{y}_0}{\omega}\sin\omega t + \frac{\gamma_y}{\omega^2}(1 - \cos\omega t) \tag{2.10}$$

$$\begin{aligned} z(t) = &(\frac{2\dot{x}_0}{\omega} - 3z_0)\cos\omega t + \frac{\dot{z}_0}{\omega}\sin\omega t + (4z_0 - \frac{2\dot{x}_0}{\omega}) + ... \\ &+ \frac{2}{\omega^2}\gamma_x(\sin\omega t - \omega t) + \frac{\gamma_z}{\omega^2}(1 - \cos\omega t) \end{aligned} \tag{2.11}$$

deriving the equations above, the velocities are also determined at each instant,

$$\begin{aligned}\dot{x}(t) = &(\frac{4\dot{x}_0}{\omega} - 6z_0)\omega_0 \cos\omega t + 2\dot{z}_0 \sin\omega t + (6\omega z_0 - 3\dot{x}_0) + ... \\ &+ \frac{2}{\omega}\gamma_z(1 - \cos\omega t) + \gamma_x(\frac{4}{\omega}\sin\omega t - 3t)\end{aligned} \tag{2.12}$$

$$\dot{y}(t) = -y_0\omega \sin\omega t + \dot{y}_0 \cos\omega t + \frac{\gamma_y}{\omega}\sin\omega t \tag{2.13}$$

$$\begin{aligned}\dot{z}(t) = &-(\frac{2\dot{x}_0}{\omega} - 3z_0)\omega \sin\omega t + \dot{z}_0 \cos\omega t + ... \\ &+ \frac{2}{\omega}\gamma_x(\cos\omega t - 1) + \frac{\gamma_z}{\omega}\sin\omega t\end{aligned} \tag{2.14}$$

2.3 Attitude equation of motions

2.3.1 Spacecraft attitude dynamics

To define the attitude dynamics, the rigid body equation of motion is given by,

$$\dot{h}_{tot} = N_e - \omega \times h_{tot} \tag{2.15}$$

The equation above is also known as Euler's equation and the term $h_{tot} = \sum_{i=1}^{N}(I_i\omega_i)$ is the sum of the angular momentum of all the N rotating parts of the satellite. N_e is the sum of all the external torques acting on the spacecraft and ω is the angular velocity. All the quantities are expressed in the body reference frame. For the attitude control three reaction wheels are used, each positioned along the principal axes of the spacecraft. Thus, in this case, the chaser has a total angular momentum which depends on its inertia matrix, I_s, and the reaction wheels angular momentum, h_w. The satellite inertia matrix, I_s, is a 3×3 matrix and it is in general expressed as

$$I_s = \begin{bmatrix} I_x & -I_{xy} & -I_{xz} \\ I_{yx} & I_y & -I_{yz} \\ -I_{zx} & -I_{zy} & I_z \end{bmatrix} \tag{2.16}$$

The matrix above is symmetric and I_{xy}, I_{xz}, I_{yz} are the products of inertia, while I_x, I_y, I_z are the moments of inertia. Here, it is considered a simple case where the body frame axes coincide with the principal axes of inertia, which means it can be simplified as

$$I_s = \begin{bmatrix} I_x & 0 & 0 \\ 0 & I_y & 0 \\ 0 & 0 & I_z \end{bmatrix} \tag{2.17}$$

The Euler's equation can be then expanded as

$$\frac{d}{dt}(I_s\omega) + h_w = N_e - \omega \times I_s\omega - \omega \times h_w \tag{2.18}$$

and the angular acceleration can be expressed as

$$\dot{\omega} = I_s^{-1}N_e - I_s^{-1}(\omega \times I_s\omega) - I_s^{-1}\omega \times h_w \tag{2.19}$$

It is common to rewrite the equation replacing the cross product with a skew matrix, S(),

$$S(\omega) = \begin{bmatrix} 0 & -\omega_3 & \omega_2 \\ \omega_3 & 0 & -\omega_1 \\ -\omega_2 & \omega_1 & 0 \end{bmatrix} \tag{2.20}$$

The Euler's equation can be rewritten as

$$\dot{\omega} = I_s^{-1}N_e - I_s^{-1}(S(\omega)I_s\omega) - I_s^{-1}S(\omega)h_w \tag{2.21}$$

where $\dot{h}_w$ denotes the rate of change of the angular momentum from the reaction wheels and it is equal to the opposite of the control torque from the reaction wheels,

$$\dot{h}_w = N_c \tag{2.22}$$

2.3.2 Spacecraft attitude kinematics

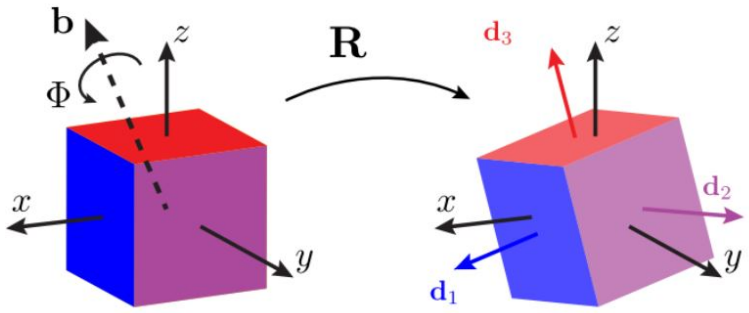

Figure 2.6: Quaternion rotation [22].

The spacecraft kinematics description is based on quaternions. The use of quaternions instead of Euler's angles to compute angular rotations results particularly convenient to avoid singularities and to reduce the computational effort of

integration in time. The quaternions are commonly defined as a 4×1 matrix

$$q = \begin{bmatrix} q_0 \\ q_1 \\ q_2 \\ q_3 \end{bmatrix} \tag{2.23}$$

where it is present a scalar part, q_0, and a vectorial part, $[q_1, q_2, q_3]^T$. A property of quaternions is that the unit quaternion must satisfy the following

$$q_0^2 + q_1^2 + q_2^2 + q_3^2 = 1 \tag{2.24}$$

and it can be also express as $q^T q = 1$ which represents a rotation. The kinematics of the spacecraft can then be expressed as

$$\begin{bmatrix} \dot{q_0} \\ \dot{q_1} \\ \dot{q_2} \\ \dot{q_3} \end{bmatrix} = \frac{1}{2} \begin{bmatrix} 0 & \omega_3 & -\omega_2 & \omega_1 \\ -\omega_3 & 0 & \omega_1 & \omega_2 \\ \omega_2 & -\omega_1 & 0 & \omega_3 \\ -\omega_1 & -\omega_2 & -\omega_3 & 0 \end{bmatrix} \begin{bmatrix} q_1 \\ q_2 \\ q_3 \\ q_4 \end{bmatrix} \tag{2.25}$$

it is possible to rewrite the equation above in a compact way as,

$$\dot{q} = \frac{1}{2} \Omega(\omega) q \tag{2.26}$$

When an attitude control is implemented the quaternions computed at each instant, from (2.25), representing the current orientation, must be compared and subtracted to the desired set of quaternions. To do so, it is convenient to introduce the expressions of some operations between quaternions. The quaternion error defines the rotation needed to get from an initial orientation to a final one. To obtain the error it is actually required the use of the quaternion product,

$$q_e = q_{des}^{-1} \otimes q_{true} \tag{2.27}$$

where the inverse of a quaternion is expressed as

$$q_d = q_{des}^{-1} = \frac{[q_0, -q_1, -q_2, -q_3]^T}{q^T q} \tag{2.28}$$

The quaternion multiplication to find the error can then be written in this way

$$q_e = q_d \otimes q_{true} = \begin{bmatrix} q_{d0} & -q_{d1} & -q_{d2} & -q_{d3} \\ q_{d1} & q_{d0} & -q_{d3} & q_{d2} \\ q_{d2} & q_{d3} & q_{d0} & -q_{d1} \\ q_{d3} & -q_{d2} & q_{d1} & q_{d0} \end{bmatrix} \begin{bmatrix} q_{true0} \\ q_{true1} \\ q_{true2} \\ q_{true3} \end{bmatrix} \tag{2.29}$$

As seen for the Euler's angles, it is possible to use quaternions as well to define a rotation matrix between the orbit frame and the body frame

$$L^B_{LVLH} = \begin{bmatrix} q_0^2 + q_1^2 - q_2^2 - q_3^2 & 2(q_1q_2 - q_3q_0) & 2(q_1q_3 + q_2q_0) \\ 2(q_1q_2 + q_3q_0) & q_0^2 - q_1^2 + q_2^2 - q_3^2 & 2(q_2q_3 - q_1q_0) \\ 2(q_1q_3 - q_2q_0) & 2(q_2q_3 + q_1q_0) & q_0^2 - q_1^2 - q_2^2 - q_3^2 \end{bmatrix} \tag{2.30}$$

Quaternions are not visually intuitive so at the end they are usually converted back in Euler's angles to better understand the rotation

$$\begin{aligned} \phi &= \arctan\left(\frac{2(q_0q_1 + q_2q_3)}{q_0^2 + q_1^2 - q_2^2 - q_3^2}\right) \\ \theta &= \arcsin\left(-2(q_1q_3 + q_0q_2)\right) \\ \psi &= \arctan\left(\frac{2(q_1q_2 + q_0q_3)}{q_0^2 - q_1^2 - q_2^2 + q_3^2}\right) \end{aligned} \tag{2.31}$$

2.3.3 Actuation, Reaction Wheels

A Reaction wheel is a device which is used in order to control the attitude of a spacecraft. It consists of a wheel built to have a large inertia and a low mass, which is connected to an electric motor. As any other forms of actuation in space, it is based on momentum exchange and in particular a reaction wheel redistributes the momentum within the satellite body. The wheel produces a torque along its axis, so to enable a full attitude control at least three of them are required. The main advantage of reaction wheels is that they do not consume propellant. They only need energy for the DC motor which a battery can provide. The battery can be then simply recharged by the solar panels. Reaction wheels are commonly controlled in terms of torque and velocity. In fact, they can reach saturation both in terms of torque and velocity. Each reaction wheel is connected to an electric motor which is able to generate a desired torque and to transmit it to the reaction wheel. The latter will then produce an equal and opposite torque on the motor (Newton's third law) which will start to spin in the opposite direction with the entire spacecraft. The torque saturation happens when the couple required is bigger than the one that the motor is able to produce. In the specific case of an electric motor it means too much current is asked. This problem is avoided with a correct design of the reaction wheel. Hence, to obtain a torque the disk has to accelerate which means that during its life the reaction wheel increases the rotation velocity until the friction acting on the motor becomes too big, and velocity saturation occurs. At this point the reaction wheel must be stopped and discharged. To avoid that during this operation the satellite changes the attitude, counteractions must

be taken: commonly thrusters or magnetorquers. In the paragraph below, the torque coming from the reaction wheel is derived.

Reaction Wheels control loop

Consider a single reaction wheel having a given inertia, I_w, and with an angular velocity ω_w. Based on this information it can be determined the torque acting on the disk from the motor

$$N_w = \dot{h} = \frac{d}{dt}(I_w \omega_w) \tag{2.32}$$

This means that the torque acting on the spacecraft will be the opposite based on what has been said before. The control torque, N_c, is equal to the actuation torque coming from the reaction wheel, N_w,

$$N_c = -N_w \tag{2.33}$$

Until now a simplified case has been considered while in reality a control torque has a limited bandwidth and the control loop is defined by a low-pass filter between N_c and N_w,

$$\tau_w \ddot{h} = -\dot{h} + N_w \tag{2.34}$$

$$N_c = -\dot{h} \tag{2.35}$$

$$h(t) = \int_0^t h(\tau) d\tau + h(0) \tag{2.36}$$

From the equations above the low-pass filter is obtained in frequency domain,

$$N_c = -\frac{1}{1 + s\tau_w} N_w \tag{2.37}$$

To be able to fully control the attitude of a spacecraft, at least one reaction wheel for each axis is needed. To derive the total contribution, a 3D model must be consider. The direction along which the reaction wheels are oriented can differ from the axis of the body frame so a rotation matrix has to be used. Using a vectorial form the full model for a total number of n_{wheel} can be defined

$$\begin{aligned} N_w &= \begin{bmatrix} N_{w_1} & N_{w_2} & ... & N_{w_{n_{wheel}}} \end{bmatrix} \\ h_w &= \begin{bmatrix} h_{w_1} & h_{w_2} & ... & h_{w_{n_{wheel}}} \end{bmatrix} \\ \omega_w &= \begin{bmatrix} \omega_{w_1} & \omega_{w_2} & ... & \omega_{w_{n_{wheel}}} \end{bmatrix} \end{aligned} \tag{2.38}$$

Figure 2.7: 3-axis reaction wheels for CubeSats and DC motor [23].

A transformation matrix $L_w^B \in \Re^{3\times n_{wheel}}$ is considered to pass from the reaction wheels reference frame to the body frame. Finally, it can be written

$$\begin{aligned} N_{w_B} &= L_w^B N_w \\ h_{w_B} &= L_w^B h_w \end{aligned} \tag{2.39}$$

In this research, a 3D model with three reaction wheels aligned along the body axis is developed. In this case, L_w^B becomes a 3×3 identity matrix.

2.4 Rendezvous and Proximity Operation Maneuver

In this section a brief description of the most common ideal maneuvers for rendezvous and proximity operations is presented and their respective accelerations and ΔVs are reported. This description is useful for a better understanding of the relative motion of the chaser with respect to the target and of the performance of the different maneuvers. The trajectories described below are later used to build the entire maneuver of the mission. These maneuvers are developed in an ideal case without considering the effect of disturbances. It is possible to find more information in this reference [3].

Tangential Boost Maneuvers

The chaser starts a transfer along the V-bar when a tangential boost is fired. In fact if the ΔV is generated in the same verse of the velocity (a positive boost), then

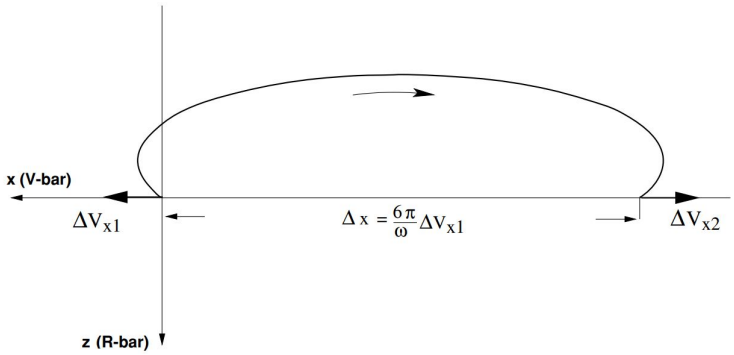

Figure 2.8: V-bar impulsive maneuver [3].

the spacecraft accelerates and rises on a higher orbit, while also moving away from the target. The opposite happens with a negative ΔV where the chaser instead gets closer to the target. So after an entire orbit period T the chaser translates of a distance equal to

$$\Delta x = \frac{6\pi}{\omega}\Delta V_x \tag{2.40}$$

where $\omega = \frac{2\pi}{T}$ is the target angular velocity. The ΔV_x must be generated two times, once at the start and once at the end to stop the maneuver. Of course, based on the amount of ΔV generated, the spacecraft will be able to cover a bigger or smaller longitudinal space. The total ΔV required is then

$$\Delta V = \frac{\omega}{3\pi}\Delta x \tag{2.41}$$

If the maneuver is instead just stopped after half an orbit period, then it can be used in order to get a spacecraft from a starting orbit to a final orbit at a different altitude. The maneuver can be executed with an impulsive thrust along the x axis at the beginning and then at the end to stop the spacecraft once the final orbit has been reached. This maneuver is famously known as a Hohmman transfer and it only lasts half the time than the previous one [3].

There is a fixed relation between the distance traveled along the x-axis and z-axis with a Hohmann transfer

$$\Delta x = \frac{3\pi}{4}\Delta z \tag{2.42}$$

This expression can be used in (2.41) to find the cost of each tangential boost. The cost in ΔV is the same at the start and the end in the approximation of the CW equations, for small changes in altitude. Once the final position is reached and the maneuver stopped, the chaser will keep moving only of a free drift motion.

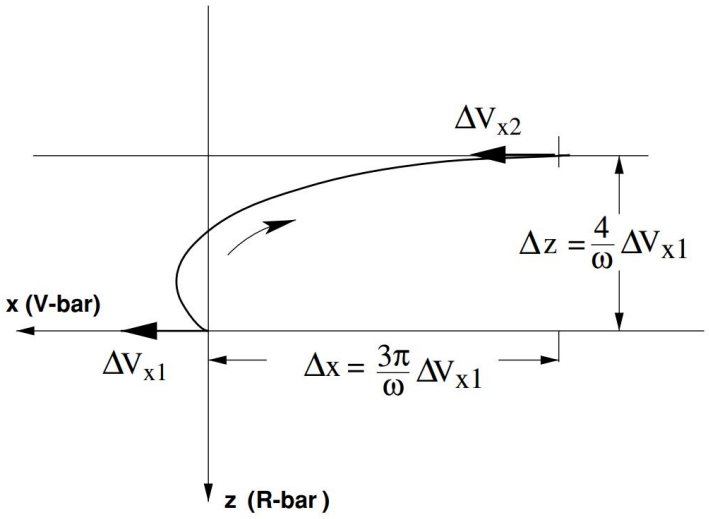

Figure 2.9: Impulsive Hohmann transfer [3].

Here a CubeSat mission is considered and the thrust which a nanosatellite is able to generate is limited. So, instead of an high impulsive boost at the beginning and at the end of the maneuver, it is thought instead to apply a continuum thrust through all the Hohmann transfer.

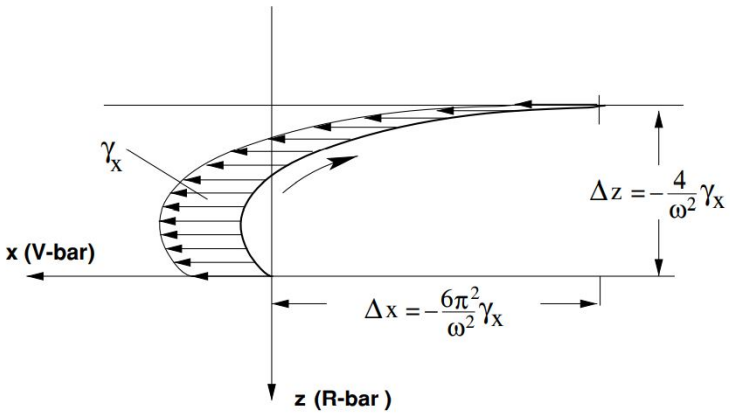

Figure 2.10: Continuous acceleration along V-bar [3].

The ΔVs are still the same for the continuous and impulsive maneuver but the continuous one needs double the time to complete the transfer. Hence, the thrust per unit mass needed is then,

$$\gamma_x = -\frac{\omega^2}{4\pi}\Delta z \tag{2.43}$$

This unit thrust operates for an entire period, T, to get the spacecraft to the final position and once the target point is reached the acceleration is set to zero, $\gamma_x = 0$, and the maneuver stops. The ΔV can be derived as

$$\Delta V = \gamma_x T = \frac{\omega}{2}\Delta z \tag{2.44}$$

Radial Boost Maneuver

A widely used maneuver to approach a target on the same orbit of the chaser is to thrust along the radial direction. In its impulsive formulation a first boost is required to start the maneuver and one at the end to stop the motion [**feshe**].

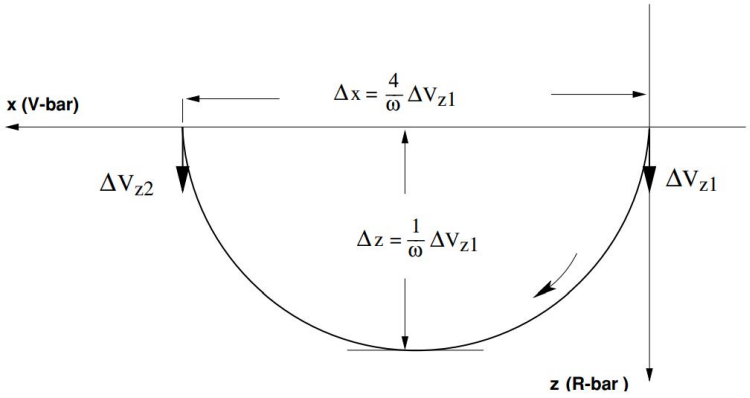

Figure 2.11: Impulsive boost along R bar [3].

This maneuver requires half an orbit period to be executed and the cost for each boost is shown in the following expression

$$\Delta V = \frac{\omega}{4}\Delta x \tag{2.45}$$

It can be noticed from the equation above that the maneuver cost changes as a function of the translation required along the V-bar. As for the previous case the maneuver can be also continuous if needed for thrust limitations and in this case the maneuver lasts an entire orbit period.

The actual unit thrust that has to be fired in this case is then,

$$\gamma_z = \frac{\omega^2}{4\pi}\Delta x \tag{2.46}$$

where Δx is the shift needed along x axis. From here considering that the maneuver is accomplished in one period time, the ΔV is,

$$\Delta V = \gamma_z T = \frac{\omega}{2}\Delta x \tag{2.47}$$

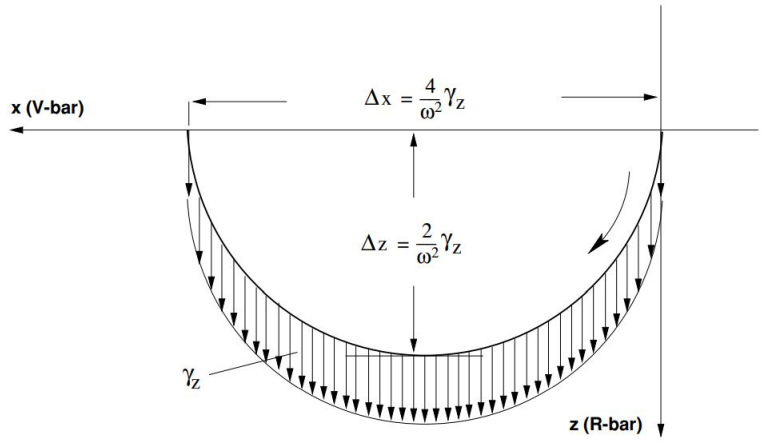

Figure 2.12: Continuous boost along R bar [3].

This maneuver is particularly interesting if compared to other similar trajectories do to safety reasons.

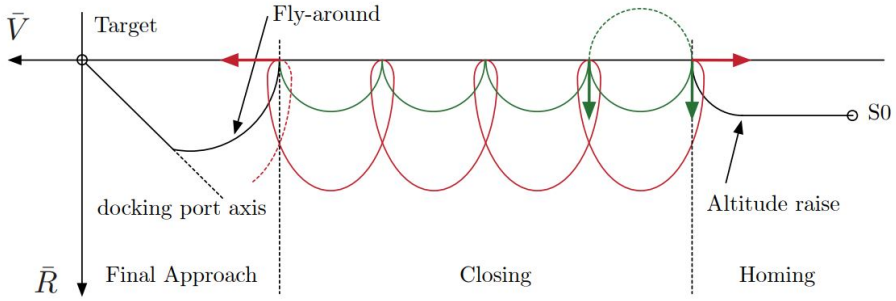

Figure 2.13: Comparison between tangential and radial maneuvers [8].

As depicted in Fig. 2.13, a closing phase along the target orbit can be usually executed with a tangential or a radial maneuver. In the tangential case, a ΔV is generated along the V-bar to start the maneuver. Once the chaser begins the approach, it will not stop until a second ΔV equal and opposite to the first one is executed. This behaviour creates a possible safety issue because in case of full or partial malfunction from the thrusters, the chaser will not be able to stop with the consequent risk of collision. The radial boost instead allows an higher level of safety because if a failure happens the chaser does not continue the closing but it remains on a passive orbit at a constant distant from the target. The main disadvantage of this maneuver is the cost. In fact it requires a ΔV which is $\frac{3\pi}{2}$ times bigger than the one needed by a tangential transfer. Many examples of real closing phase maneuvers, such as for ATV, HTV, SSO, show that in general it is

preferable to accept a more expensive maneuver but safer.

2.5 Environmental Disturbances

2.5.1 Aerodynamic Torque

The Earth is surrounded by a layer of air and its density decreases while moving further from the planet surface. The air produces aerodynamic resistance on the spacecraft which can cause orbit lowering and ultimately decay. The contribution of the aerodynamic drag depends strongly from the altitude. In fact spacecrafts, which operate in LEO, are mainly affected by aerodynamic resistance due to the still high density of air, while its contribution tends to lose importance with the orbit radius increase. A typical expression for the aerodynamic force is

$$F_D = \frac{1}{2}\rho V^2 S C_D \hat{V} \tag{2.48}$$

where ρ is the air density at the orbit altitude, V is the relative velocity of the spacecraft respect to the atmosphere, S is the spacecraft surface perpendicular to the velocity vector and $C_D = 2.2$ for a LEO orbit is the drag coefficient. Out of simplicity the surface is considered constant but, in reality, it depends from the orientation of the spacecraft with respect to the velocity vector. If the aerodynamic force is expressed in the orbital reference frame and the orbit is circular, then the unit vector, $\hat{V}$ can be defined as

$$\hat{V} = \begin{bmatrix} -1 \\ 0 \\ 0 \end{bmatrix} \tag{2.49}$$

In fact the aerodynamic force always acts parallel to the velocity, which is tangent to the the orbit, and in the opposite direction. The drag force can in general causes a disturbance torque in presence of an offset between the spacecraft center of mass and the aerodynamic center of pressure. The latter is the point where the aerodynamic force acts on the spacecraft. The result is a torque which can be written as

$$T_a = r_{cp} \times F_D \tag{2.50}$$

2.5.2 Magnetic Torque

One of the most significant disturbances in LEO is the magnetic torque. This effect is often used, especially on CubeSats, to actively orientate the spacecraft using magnetic coils, also known as magnetorques. However, also electronic devices and

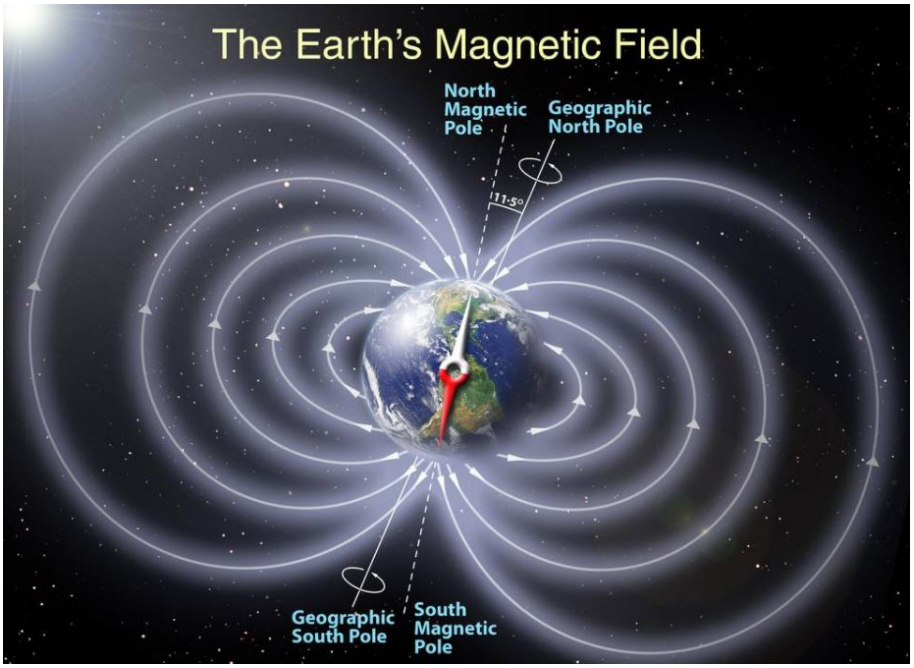

Figure 2.14: Earth magnetic field [24].

ferromagnetic materials on board of the spacecraft create a magnetic field which is able to interact with the Earth magnetic field, generating a torque acting on the spacecraft and changing its attitude. This contribution must be considered to guarantee an adequate attitude control. The magnetic torque can be expressed as

$$T_m = m \times B \tag{2.51}$$

where B is the Earth magnetic field and m is the residual dipole.
The Earth presents a magnetic south pole which is around 11.5° below the geographic north pole and a magnetic north pole, close to the south pole. The Earth magnetic field has a quite complex distribution. It decreases with the distance and, especially at high altitudes, it is strongly influenced by the solar magnetic field and by the occasional solar events. The magnetic poles are also not fixed in their positions, but tend to move, changing the magnetic field distribution. The International Geomagnetic Reference Field (IGRF) model is typically applied to determine the value of the magnetic field in the surrounding of the Earth. This model is periodically updated to consider the continuous variations in the field. It can be expressed as

$$V(r,\phi,\theta,t) = a\sum_{n=1}^{k}\left(\frac{a}{r}\right)^{n+1}\sum_{m=0}^{n}(g_n^m\cos m\phi + h_n^m \sin m\phi P_n^m(\theta)) \tag{2.52}$$

where θ is the latitude minus 90°, ϕ the longitude, r the distance from the Earth and a the equatorial radius. g_n^m and h_n^m are the Gaussian coefficients, and P_n^m is the Schmidt function. This model is very accurate but also quite complicated, so in this research a simplified dipole model [25] is considered to describe the Earth magnetic field

$$B = \begin{bmatrix} B_1 \\ B_2 \\ B_3 \end{bmatrix} = \frac{\mu}{r^3} \begin{bmatrix} \cos \omega_0 t \sin i_m \\ -\cos i_m \\ 2 \sin \omega_0 t \sin i_m \end{bmatrix} \tag{2.53}$$

where μ is the field dipole strength, r is the orbit radius, i_m is the orbit inclination with respect to the magnetic equator and $\mu = 7.9 \times 10^{15} Wbm.$ is the dipole strength of the field.
The residual dipole moment is not commonly known for a spacecraft. To obtain precise values of this field, it is necessary to build the system at first and then measure it in a lab. In an initial phase then, an estimate must be done. Based on the results in [26], for a 3U CubeSat can be considered a residual dipole of around 0.1 Am^2.

2.5.3 Gravity Gradient

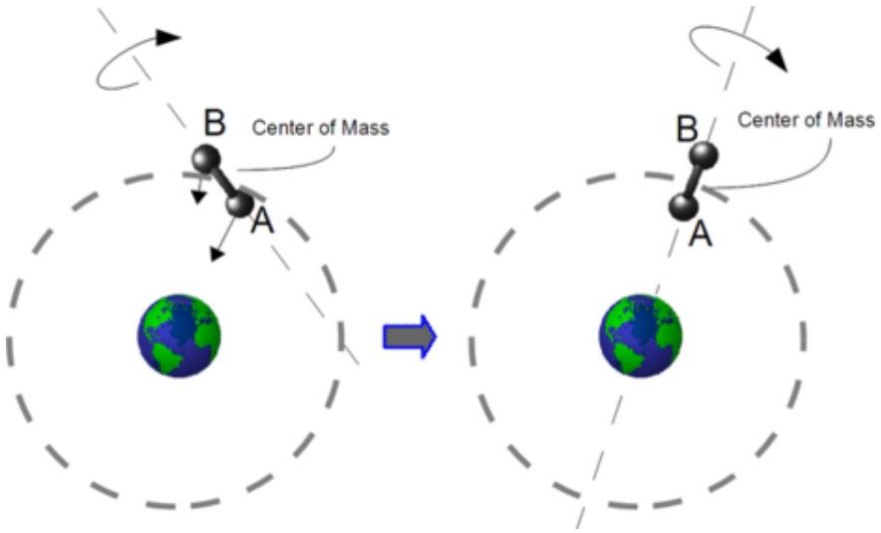

Figure 2.15: Gravity gradient effect [27].

The Earth is a geoid with a non uniform distribution of mass, so the gravity field potential has a quite complicate expression in reality. However as a first approximation the Earth can be considered a sphere with a homogeneous distribution

of mass. This makes the gravitational field uniform and easy to study. According to Newton's gravitational law, the gravitational force reduces with the square of the distance, so a spacecraft will experience an higher force at the extremity closer to the planet, while a smaller one at the extremity further away. This effect can produce a torque acting on the spacecraft. In fact the torque will change its attitude trying to align the minimum inertia axis along the gravitational field direction. It has to be noticed that this couple is present only if the principal moment of inertia are unequal. The gravity-gradient torque is typically expressed as

$$T_g = \frac{3\mu}{r^3}\hat{r} \times [I]\hat{r} \tag{2.54}$$

where μ is the Earth gravitational parameter, r is the distance of the spacecraft from the Earth center of gravity and I is the principal moment of inertia.

Chapter 3

Guidance and Control System Design

In this chapter two algorithms are described: a ZEM-ZEV guidance and an LQR controller. The first is referred to the long-range mission and the second is developed for the short-range mission. The focus is on the implemented algorithms, after a general introduction to the theories.

3.1 Zero-Effort-Mission/Zero-Effort-Velocity

3.1.1 Classic ZEM-ZEV

The Zero-Effort-Mission/Zero-Effort-Velocity (ZEM-ZEV) is a feedback guidance law widely known and studied for its analytical simplicity and its robustness against external perturbations. It has been particularly successful for applications like missile guidance and planetary landing, where the gravitational field can be considered constant and the ZEM-ZEV can give an energy optimal solution. The objective of this law is to guide a spacecraft with a certain initial position and velocity to a final aim point. Usually, the equations can be developed both in a relative or inertial reference frame fixed within the target. The control acceleration computed by the ZEM-ZEV algorithm is classically defined as

$$a = \frac{6}{t_{go}^2} ZEM - \frac{2}{t_{go}^2} ZEV \tag{3.1}$$

where t_{go} is the so called time-to-go. This variable defines the difference between the final time, at the end of the trajectory, and the elapsed time from the start of

the maneuver, and it is expressed as

$$t_{go} = t_f - t \tag{3.2}$$

As all the other optimal feedback guidance algorithms, also the ZEM-ZEV is optimal for a specific time duration of the maneuver. In many applications, such as asteroid interceptions, it is not important the time needed to reach the target, so for these cases the optimal time of flight can be applied. The computation of the optimal flight duration is not trivial though: it requires to find the minimum of the performance index with respect to the time-to-go [28]. Once the t_{go} has been determined it can be used as an input to find the control acceleration. If instead the time of flight is of specific interest, then it can be fixed to the desired value, but this means that more fuel will be consumed to slow down or speed up the chaser during the approach in order to reach the target at the required time.

Another reason why this parameter is particularly relevant and problematic in the computation of the control accelerations is that, as the elapsed times grows, the time-to-go gets smaller causing a considerable increase of the control signal which can tend to infinite. So it is important to pay particular attention while choosing the t_{go} value, in order to avoid a consequent high fuel consumption.

The ZEM distance is defined as the difference between the desired final position and the predicted final position if no acceleration is applied to the spacecraft. In a similar way the ZEV is the error between the desired and the actual velocity at the final instant, $t = t_f$, if no control action is applied. They are commonly formulated as

$$ZEM = r - \tilde{r}_f \tag{3.3}$$

$$ZEV = v - \tilde{v}_f \tag{3.4}$$

In the equations above for the ZEM and ZEV, the expressions of the predicted final position, $\tilde{r}$, and velocity, $\tilde{v}$, can be rewritten. To do so the dynamic equations of motion are considered in an inertial reference frame, if no control action is applied

$$\dot{r} = v$$

$$\dot{v} = g$$

where g is the gravitational force, while r and v are the position and velocity of the chaser. So knowing the initial conditions at the time t, the dynamic equations

above are integrated to find the position, $\tilde{r}_f$, and velocity , $\tilde{v}_f$, at the defined final time, t_f. Substituting in the the ZEM and ZEV expressions, it is possible to derive

$$ZEM = r_f - [r + t_{go}v + \int_t^{t_f} (t_f - \tau)g(\tau)\, d\tau] \tag{3.5}$$

$$ZEV = v_f - [v + \int_t^{t_f} g(\tau)\, d\tau] \tag{3.6}$$

where $g(\tau)$ is the gravitational field of the target as a function of time. Its intensity depends on the target mass and it can be omitted if it is sufficiently small, like for an asteroid or for a spacecraft rendezvous.

The ZEM-ZEV is not in general an optimal guidance law, but it becomes so if the gravitational field is uniform or if it varies only as a function of time. In these cases the optimal time-to-go can be computed for the maneuver. In reality though, most of the time, the gravitational field in the equations depends also on the position, $g(x, t)$, like during a transfer maneuver. Then the optimal time-to-go can not be found and the guidance is not an optimal law. In some cases though, near-optimal results can be achieved introducing waypoints along the trajectory, as it is discussed in the next paragraph.

3.1.2 Modified ZEM-ZEV

The classical formulation of the ZEM-ZEV is modified to be adapted to the problem of rendezvous. As previously seen, in the classical guidance formulation the final position and velocity to reach are fixed and compared with the predicted final position and velocity, while the t_{go} is computed with respect to the expected final maneuver time. Following this approach it would not be possible to control the shape of the trajectory and the accelerations could grow significantly. In fact the classic ZEM-ZEV, based on the initial conditions, will produce a correction acceleration to guide the chaser to the desired final conditions but, doing so, the spacecraft will start moving on a different path from the one desired. If, for example, the spacecraft starts the maneuver from a lower orbit respect to the target, it will have an initial free drift velocity along the V-bar. Imagining to execute a Hohmann transfer to reach the target orbit, then the ZEM-ZEV guidance, in order to accomplish the approach, will compute at first an acceleration command to reduce the velocity along the V_{bar} and one to rise the chaser up along the R_{bar}. The result is a trajectory much different from the desired one.

Hence, instead of having as a reference the final station keeping points for each segment of the whole maneuver, a time-to-go of only a fraction of seconds is considered. As a result the aimed position will be a waypoint not much far from the current position.

The scenario considered in this work is a rendezvous between two CubeSats and for this reason the effect of the gravitational field acting on the chaser can be neglected. So the expressions of the ZEM and ZEV errors can be simplified as

$$ZEM = r - \tilde{r}_f = r_f - r + t_{go}v \tag{3.7}$$

$$ZEV = v - \tilde{v}_f \tag{3.8}$$

In order to find the desired position, r, and velocity, v, in the relations above, the Clohessy-Wiltshire equations are considered. Following a similar approach as in [15], the position can be expressed as

$$\begin{aligned} x(t) = {} & A_x \sin\omega t - \cos\omega t + C_x t + D_x + ... \\ & + E_x(\omega t - \sin\omega t) + F_x(\frac{4}{\omega^2}(1 - \cos\omega t) - \frac{3}{2}t^2) \end{aligned} \tag{3.9}$$

$$y(t) = A_y \cos\omega t + B_y \sin\omega t + C_y(1 - \cos\omega t) \tag{3.10}$$

$$\begin{aligned} z(t) = {} & A_z \cos\omega t + B_z \sin\omega t + C_z + ... \\ & + D_z(\sin\omega t - \omega t) + E_z(1 - \cos\omega t) \end{aligned} \tag{3.11}$$

and in a similar way the velocity are

$$\begin{aligned} \dot{x}(t) = {} & A_x\omega_0 \cos\omega t + B_x\omega \sin\omega t + C_x + ... \\ & + E_x\omega(1 - \cos\omega t) + F_x(\frac{4}{\omega}\sin\omega t - 3t) \end{aligned} \tag{3.12}$$

$$\dot{y}(t) = -A_y\omega \sin\omega t + B_y\omega \cos\omega t + C_y\omega \sin\omega t \tag{3.13}$$

$$\begin{aligned} \dot{z}(t) = {} & -A_z\omega \sin\omega t + B_z\omega \cos\omega t + ... \\ & + D_z\omega(\cos\omega t - 1) + E_z\omega \sin\omega t \end{aligned} \tag{3.14}$$

where the coefficients $A_x, B_x, C_x, D_x, E_x, F_x, A_y, B_y, C_y, A_z, B_z, C_z, D_z, E_z$, are defined as the following

$$
\begin{aligned}
A_x &= (\frac{4\dot{x}_0}{\omega} - 6z_0) \\
B_x &= \frac{2\dot{z}_0}{\omega} \\
C_x &= (6\omega z_0 - 3\dot{x}_0) \\
D_x &= (x_0 + 2\frac{z_0}{\omega}) \\
E_x &= \frac{2}{\omega^2}\gamma_z \\
F_x &= \gamma_x
\end{aligned}
$$

$$
\begin{aligned}
A_y &= y_0 \\
B_y &= \frac{\dot{y}_0}{\omega} \\
C_y &= \frac{\gamma_y}{\omega^2} \\
A_z &= (\frac{2\dot{x}_0}{\omega} - 3z_0) \\
B_z &= \frac{\dot{z}_0}{\omega} \\
C_z &= (4z_0 - \frac{2\dot{x}_0}{\omega}) \\
D_z &= \frac{2}{\omega^2}\gamma_x \\
E_z &= \frac{\gamma_z}{\omega^2}
\end{aligned}
$$

The accelerations γ_x, γ_y and γ_z in the Clohessy-Wiltshire equations are the one derived for the ideal case and computed in the relations (2.43) and (2.46). These in fact, as specified before, are the accelerations needed to follow the desired trajectory for an open-loop. The resultant position and velocity from the equations are treated as the final position and velocity to reach. The Clohessy-Wiltshire equations are a function of time. In order to obtain correct results the time used in the equations must have the following expression

$$t = (t_{sim} - t_{0_i}) + t_p \tag{3.15}$$

where the simulation time, t_{sim}, is the time from the start of the simulation, t_{0_i} is the time at which the current part of the maneuver starts, and t_p is the prediction

time. Hence, the time considered in Eq.(3.15) is the elapsed time from the last station keeping point where the current trajectory is started, plus the prediction time which coincides with the defined time-to-go. As seen in the last chapter a rendezvous maneuver is developed using different types of trajectories, such as a Hohmann transfer or a radial boost approach. Thus, at the beginning of each of these phases is necessary to change the initial conditions before running the guidance algorithm, and t_{0_i} must restart from zero at each station-keeping point.

The predicted position, $\tilde{r}$, and velocity, $\tilde{v}$, are again estimated from the Clohessy-Wiltshire equations but here the ideal accelerations, γ_x, γ_y and γ_z, are neglected and the actual position and velocity are propagated of t_{go} if any control acceleration is acting on the spacecraft. Thus, as for the ideal case the equations of relative motion are implemented

$$x(t) = A_x \sin(\omega\Delta t) - \cos(\omega\Delta t) + C_x\Delta t + D_x \tag{3.16}$$
$$y(t) = A_y \cos(\omega\Delta t) + B_y \sin(\omega\Delta t) \tag{3.17}$$
$$z(t) = A_z \cos(\omega\Delta t) + B_z \sin(\omega\Delta t) + C_z \tag{3.18}$$
$$\tag{3.19}$$

and in a similar way the velocities are

$$\dot{x}(t) = A_x\omega_0 \cos(\omega\Delta t) + B_x\omega \sin(\omega\Delta t) + C_x \tag{3.20}$$
$$\dot{y}(t) = -A_y\omega \sin(\omega\Delta t) + B_y\omega \cos(\omega\Delta t) \tag{3.21}$$
$$\dot{z}(t) = -A_z\omega \sin(\omega\Delta t) + B_z\omega \cos(\omega\Delta t) \tag{3.22}$$
$$\tag{3.23}$$

The time variation, Δt, in the equations above is the propagation time from the current time. This time exactly corresponds to the time-to-go. As a result, from these equations the position and velocity of the chaser propagated in time of t_{go}, if no control acceleration is applied, are obtained.
It is now possible to compute the ZEM and ZEV errors inserting the desired and predicted position and velocity, computed from the Clohessy-Wiltshire equations, in the relations (3.7) and (3.8), which are then used in (3.1) to find the the guidance control accelerations.

The modified ZEM-ZEV, as will be better shown in the next chapter, allows to correctly execute the rendezvous maneuver and to follow the desired trajectory. This is the result of a reduction in the propagation time, t_{go}, which significantly lowers the errors in position and velocity measured by the ZEM and ZEV respectively.

Additionally, in this way, the control acceleration from the guidance is then kept low.

3.2 Linear Quadratic Regulator

A control law, in general, has the objective to govern the input signal to drive the dynamic system to a desired final state. So with a control function it is possible to bring a spacecraft from an initial to a final state following a specific path, or to change the orientation of a satellite against external disturbances. A widely known algorithm is the linear quadratic regulator (LQR) control. This control can be only applied to linear systems, so if a non-linear system is considered, it must be linearised first. A linear or linearised system is commonly represented as a state-space system

$$\dot{x} = Ax + Bu$$
$$\dot{y} = Cx + Du$$

where

- x is named state vector, $\in \Re^m$
- y is named output vector, $\in \Re^q$
- u is named input/control vector, $\in \Re^n$
- A is named state matrix, $\in \Re^{m,m}$
- B is named input matrix, $\in \Re^{m,n}$
- C is named output matrix, $\in \Re^{q,m}$
- D is named feedthrough matrix , $\in \Re^{q,n}$

In many applications, as the one considered in this research, the system written above can be simplified, considering it as a full-state feedback. Under this condition, the matrix $[C] = I$, which is the identity matrix, and $[D] = 0$. As a result the state vector and the output vector coincide. The objective of the control is to bring the state vector to converge, but without consuming too much fuel. Hence, the ideal would be to find a balance between the fast regulation and the cost of the maneuver. A cost function is then defined

$$J = \frac{1}{2}\int_0^t [x^T Q x + u^T R u]\, dt \tag{3.24}$$

In this function, Q and R are two matrices which are used to regulate performance and cost of actuation respectively, and they are commonly known as weighting matrices. So acting on the Q matrix, it is possible to decide how aggressive is going

to be the controller response in reducing the state error. The R matrix, instead, defines the actuators effort, which translates in how much propellant is needed for the operation. On a spacecraft if thrusters are considered for the actuation, it is then preferable to increase the R matrix to save fuel. If, instead, reaction wheels are used, the energy comes from batteries charged by the solar panels, so in this case the consumption is not that relevant, while it is more important to increase the Q matrix to decrease the error control. The weighting matrices are typically diagonal, and each element can be tuned to change the relative contribution of each of them.

Once the feedback law has been defined as $u = -Kx$, the aim is to find the optimal control gain , K, which minimizes the cost function, J. The gain which allows to minimizes the cost function is so defined

$$K = R^{-1}B^T X \tag{3.25}$$

where X is a unique semi-definite solution of the Riccati equation

$$A^T X + XA - XBR^{-1}B^T X + Q = 0 \tag{3.26}$$

After the K matrix has been found, it is also important to check the stability of the system, evaluating the eigenvalues

$$\lambda = eig(A - KB) \tag{3.27}$$

The gain can be computed as a time-varying function, as it is explained in [17], so in this case the K matrix is update during the maneuver. The other option is to solve the problem off-line and keeping fixed the gain value. The first choice allows to obtain better performance and less fuel consumption but at the same time it introduces a significant increment in computation effort. In this work, the simpler second approach has been followed, in fact it is reasonable to think that a CubeSat has a limited on-board computational power.

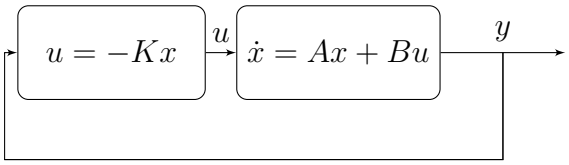

Figure 3.1: LQR block diagram for a full state feedback problem.

3.2.1 Position Control

An LQR control has been developed in this work to bring a spacecraft from an initial position and velocity to a final one, following a specified trajectory. To describe the relative motion of the chaser respect to the target, the Hill equations are implemented. They are already linear by definition, so the LQR control can be applied without problems. The state-space representation can be defined as

$$\dot{x} = Ax + Bu \tag{3.28}$$

where x is the state-space vector and it defines a error

$$x = \begin{Bmatrix} x_d \\ y_d \\ z_d \\ \dot{x} \\ \dot{y} \\ \dot{z} \end{Bmatrix} - \begin{Bmatrix} x_r \\ y_r \\ z_r \\ \dot{x} \\ \dot{y} \\ \dot{z} \end{Bmatrix} \tag{3.29}$$

which is the difference between the desired state that the chaser aim to reach and the one where the chaser actually is at the considered instant. The input to the Hill equations are the forces computed by the controller and are expressed as

$$u = \begin{Bmatrix} F_x \\ F_y \\ F_z \end{Bmatrix} \tag{3.30}$$

The components of the force are expressed in the orbital reference frame. Finally the state matrix, A, and input matrix, B, are

$$A = \begin{bmatrix} 0 & 0 & 0 & 1 & 0 & 0 \\ 0 & 0 & 0 & 0 & 1 & 0 \\ 0 & 0 & 0 & 0 & 0 & 1 \\ 0 & 0 & 0 & 0 & 0 & 2\omega \\ 0 & -\omega^2 & 0 & 0 & 0 & 0 \\ 0 & 0 & 3\omega^2 & -2\omega & 0 & 0 \end{bmatrix} \tag{3.31}$$

$$B = \frac{1}{m} \begin{bmatrix} 0 & 0 & 0 \\ 0 & 0 & 0 \\ 0 & 0 & 0 \\ 1 & 0 & 0 \\ 0 & 1 & 0 \\ 0 & 0 & 1 \end{bmatrix} \tag{3.32}$$

where ω is the target angular velocity and m is the chaser mass.
For the rendezvous maneuver six different trajectories are implemented and for each of them a different gain matrix, K, has been computed. In fact, for each trajectory, different cost matrices must be applied in order to succeed in making the LQR controller follow the desired path. A reasonable initial assumption for the cost matrix Q is the identity matrix, while R, as shown in [8], can be expressed as

$$R = \begin{bmatrix} 1/(u_{1_{max}}^2) & 0 & 0 \\ 0 & 1/(u_{2_{max}}^2) & 0 \\ 0 & 0 & 1/(u_{3_{max}}^2) \end{bmatrix} \tag{3.33}$$

where u_{max} represents the maximum thrust that the actuators are able to generate. Starting from these values the matrices can then be modified to optimize the trajectory shape and fuel consumption.

3.2.2 Attitude Control

The orientation of a spacecraft and its attitude change are described by the Euler's equations for a rigid body. These are a set of non-linear equations, so to apply an LQR control the system has to be linearised. The aim of the attitude control is to bring the state vector to zero, which means to nullify the error in angular position and velocity respect to the desired final state. As for the position control, the state-space equation is

$$\dot{x} = Ax + Bu \tag{3.34}$$

In this case though, the state vector is expressed as

$$x = \begin{Bmatrix} q_1 & q_2 & q_3 & \omega_1 & \omega_2 & \omega_3 \end{Bmatrix}^T \tag{3.35}$$

This vector is the input of the gain matrix, S, and it shows the quaternion and angular velocity error. In the state vector only the vectorial components are considered and not the scalar part. This can be explained considering that once the vectorial part is determined, the scalar part is linearly dependent from the other components, in fact the condition $\|q\| = 1$ must always stand true. The control action, instead, is given by the torques computed by the LQR, $u = -Kx$,

$$u = \begin{Bmatrix} T_x \\ T_y \\ T_z \end{Bmatrix} \tag{3.36}$$

The state matrix, A, and the input matrix, B, obtained from the Euler's equations linearisation can be expressed as

$$A = \begin{bmatrix} 0 & 0 & \omega & 1 & 0 & 0 \\ 0 & 0 & 0 & 0 & 1 & 0 \\ -\omega & 0 & 0 & 0 & 0 & 1 \\ 0 & \frac{-3\omega^2}{J_x} & 0 & 0 & 0 & \frac{(J_z - J_y)\omega}{J_x} \\ \frac{3\omega^2}{J_y} & 0 & 0 & 0 & 0 & 0 \\ 0 & 0 & 0 & \frac{(J_y - J_x)\omega}{J_z} & 0 & 0 \end{bmatrix} \tag{3.37}$$

$$B = \begin{bmatrix} 0 & 0 & 0 \\ 0 & 0 & 0 \\ 0 & 0 & 0 \\ \frac{1}{J_x} & 0 & 0 \\ 0 & \frac{1}{J_y} & 0 \\ 0 & 0 & \frac{1}{J_z} \end{bmatrix} \tag{3.38}$$

For the cost matrices a starting condition can be defined, as before. Q can be initially expressed as an identity matrix, $\mathbf{I}$, while R can be written as for the position control

$$R = \begin{bmatrix} 1/(u^2_{1RW_{max}}) & 0 & 0 \\ 0 & 1/(u^2_{2RW_{max}}) & 0 \\ 0 & 0 & 1/(u^2_{RW3_{max}}) \end{bmatrix} \tag{3.39}$$

In this case to be considered are instead the maximum torque which the reaction wheels are able to produce along each axis.

3.2.3 Discrete-time Linear Model

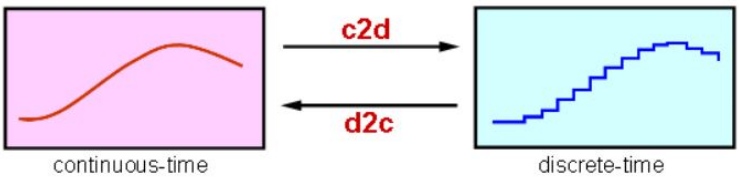

Figure 3.2: Continuous/discrete-time transformation [29].

Due to the fact that the controllers on board of a spacecraft are commonly digital, it is necessary to approximate the continuous feedback system previously defined using a discrete data model. Once the system has been discretized the feedback gain is changed so to obtain a response similar to the original one. In this research,

the sampled-data model has been obtained starting from the continuous model which has been defined before. A simple built-in MATLAB function, $c2c$, has been used for this purpose which needs three arguments: a sample time has to be chosen for the discretization of the controller, the matrices previously defined for the state-space model (A,B,C,D) and the type of hold circuit. For the latter specification the default one is left, which is a zero-order hold (ZOH) method. The MATLAB function gives as an output the discrete state-space matrices, A_k, B_k, C_k, D_k. Using these results the state-space model can be rewritten as

$$\dot{x}_{k+1} = A_k x_k + B_k u_k \tag{3.40}$$

here again is presented the case of a full-state feedback, where C_k and D_k are null matrices. Once all the matrices describing the system have been recomputed, the new gain matrix for the LQR control can be found.

Chapter 4

Simulation Results

In this chapter a brief description of the major characteristics of the spacecraft used to accomplish the rendezvous mission is provided. Then the results from the simulations are shown for each scenario, in order to validate the performance of the guidance and control algorithms previously discussed.

4.1 Spacecraft Model

Satellites can be divided in different categories based on their mass. Spacecrafts with a mass higher than 1000 kg are commonly considered large. Medium satellites are instead in a range between 1000 kg and 500 kg, while with the term small spacecrafts in general are considered all those space vehicles having a mass lower than 500 kg. If their mass is higher than 100 kg than they are called mini satellites, and if it is between 100 kg to 10 kg, they are referred to as micro satellites. The category which most of the CubeSats are part of are the nanosatellites. They range over masses between 1 kg and 10 kg. The process of miniaturization of spacecrafts went even further in the last few years, with pico and femto satellites which brought the operative mass to 0.1-1 kg and less than 0.1 kg respectively.

CubeSats are standardized nanosatellites with a unit dimension of cubic shape. This unit cube presents a dimension of $10 \times 10 \times 10$ cm and a mass of 1.33 kg. Starting from a single unit, more of these cubes can be added to obtain bigger CubeSats and carry larger payloads. In this research the rendezvous maneuver and proximity operations are exploited between two 3U CubSats. A simplified representation is shown in Fig. 4.1. Its dimensions are then of $10 \times 10 \times 10$ cm, while the mass is around 4 kg. Out of simplicity the components of the inertia matrix are evaluated with respect to the body frame, which is a principal frame, and also the CubeSat is considered as a simple rectangular prism with an homogeneous

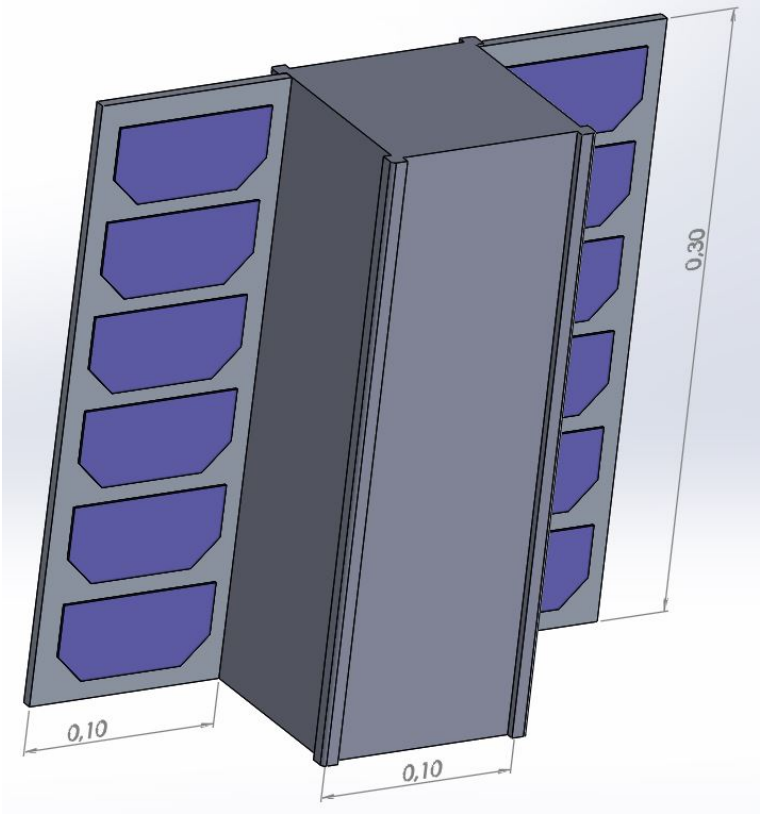

Figure 4.1: Schematic CAD representation of the chaser.

distribution of mass. It can be then expressed as

$$I = \begin{bmatrix} m\frac{a^2+b^2}{12} & 0 & 0 \\ 0 & m\frac{a^2+l^2}{12} & 0 \\ 0 & 0 & m\frac{b^2+l^2}{12} \end{bmatrix} \tag{4.1}$$

where $a = b = 10$ cm and $l = 30$ cm. The inertia values are $I_y = I_z = 0.0333$ kgm^2 and $I_x = 0.00667$ kgm^2. The solar panels contribution to the momentum of inertia is neglected in order to simplify the computation. A first estimate of their dimension is still considered to obtain more realistic results in the computation of the aerodynamic resistance and torque acting on the chaser during the maneuver. Two solar panels are applied and their dimension is posed equal to 10×30 cm each, in a similar way as in [8].

4.2 Mission Profiles

Two trajectories have been studied: a long-range maneuver and a short-range maneuver. For the first case a ZEM-ZEV guidance is developed, while the second one uses an LQR control. For the short-range scenario an attitude control is also implemented considering the action of the external disturbances. Here these missions are described. For each of them the simulation results are shown and the performance of the algorithms is evaluated.

4.2.1 Long-range Mission

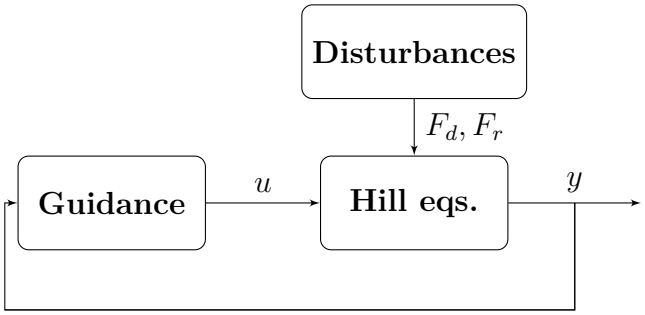

Figure 4.2: LQR, position control block diagram.

The block diagram shows a schematic representation of the simulation. The motion of the chaser is defined relative to the target, and the system is represented using the Hill equations. So this block contains the dynamic equations of motion and is the plant of the system. The input to the plant is the acceleration or force vector coming from the guidance block and the output is the actual position and velocity of the chaser at each instant. The control accelerations are computed by the ZEM-ZEV guidance which receives in input the actual position and velocity from the plant. For the simulation a block containing some of the external disturbances is also considered: here the aerodynamic drag and a random perturbation are implemented. The random disturbance is defined as 0.1 times the control acceleration from the guidance.

The maneuver is started at the first station keeping point, 11 km behind and 2 km below the target. The chaser is at first on a lower orbit respect to the target and it is drifting toward it with an initial velocity of $\frac{3}{2}wZ_0$, computed from Hill equations. Where ω is the target angular velocity and Z_0 is the chaser distance from the target in the radial direction. In the ideal case, a continuum V-bar thrust is fired to bring the chaser closer to the target and reach the final orbit. The chaser turns off the thrusters once the station keeping point S_1 is reached, 500 m behind

the target. Here the closing phase begins and a series of semicircular trajectories are followed from S_1 until the final station keeping point, S_5, is reached. These maneuvers are all executed with a continuum R-bar thrust. The approach ends with the chaser 15 m behind the target. All the station keeping points are shown in the table below.

Table 4.1: Station-keeping points in orbit frame.

SK	Definition	Position [m]
S_0	V-bar maneuver starting position	[-11456,0,2325]
S_1	V-bar maneuver final position/1° R-bar maneuver initial position	[-500,0,0]
S_2	1° R-bar maneuver final position/2° R-bar maneuver initial position	[-300,0,0]
S_3	2° R-bar maneuver final position/3° R-bar maneuver initial position	[-150,0,0]
S_4	3° R-bar maneuver final position/4° R-bar maneuver initial position	[-50,0,0]
S_5	4° R-bar maneuver final position	[-15,0,0]

In the graphs below are shown the trajectories obtained from the simulations: the homing phase from S_0 to S_1 in Fig. 4.3 and the closing phase from S_1 to S_6 in Fig. 4.4.

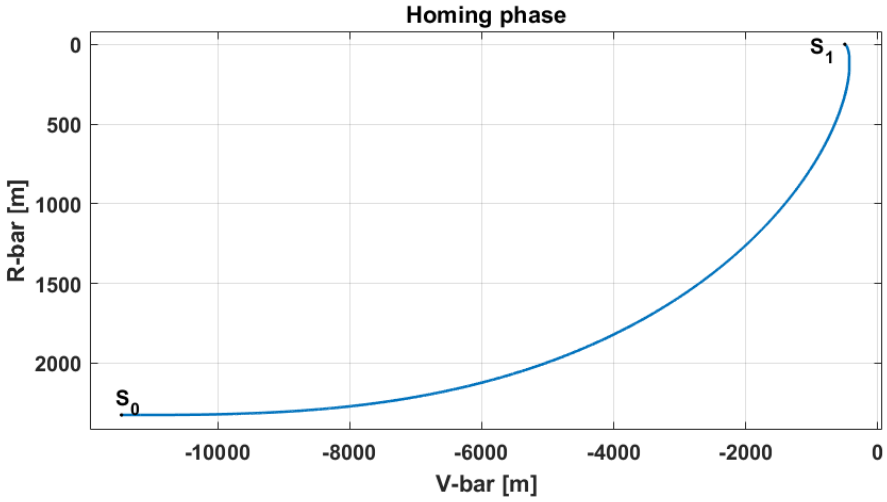

Figure 4.3: Long-range maneuver, continuum V-bar thrust trajectory.

It can be already noticed from Fig. 4.3 and 4.4 how the ZEM-ZEV shows excellent performance, in fact it is robust against the external disturbances and it

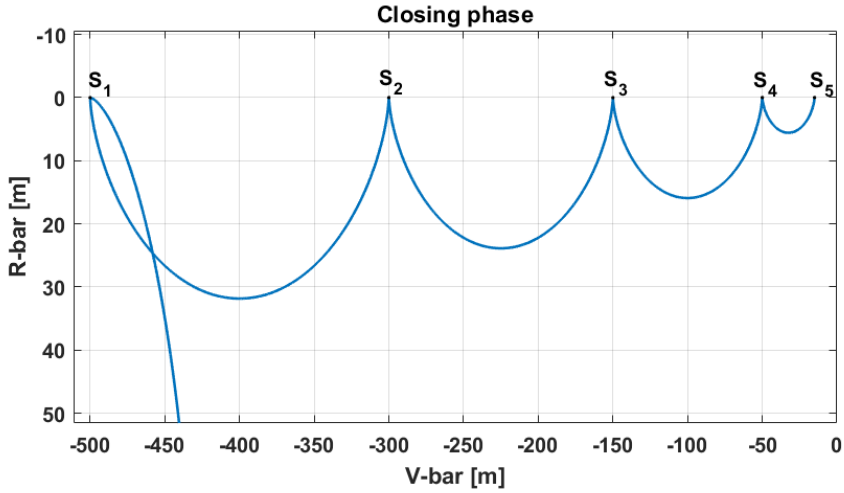

Figure 4.4: Long-range maneuver, continuum R-bar thrust trajectories.

is able to follow the desired trajectory with high precision. As it was explained in the last chapter, to make the chaser follow the desired trajectory the time-to-go must be reduced and fixed only few seconds ahead of the elapsed time.

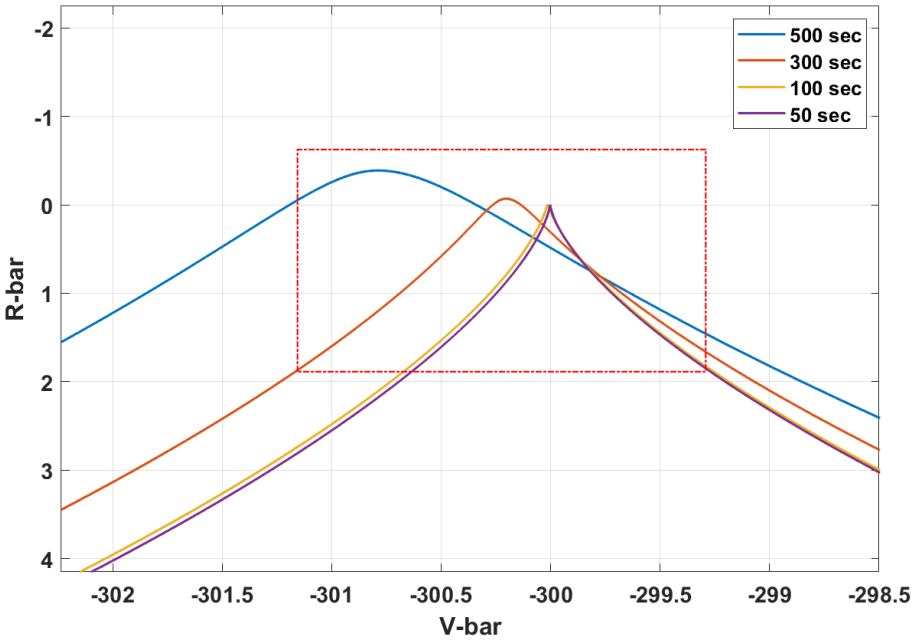

Figure 4.5: Precision in reaching a waypoint as a function of the t_{go}.

The choice of the t_{go} has in fact a direct effect on the precision of the chaser in following the trajectory. It is interesting to show this behaviour in the vicinity of a

station-keeping point. In Fig. 4.5, for example, the waypoint $S_2 = [-300, 0, 0]m$ is considered. Different values of t_{go} are chosen for each simulation, and what can be observed is that the t_{go} has a direct effect on the precision in reaching the final state. In fact a lower t_{go} guarantees a smaller error, but at the same time, more time is needed for the computation. So, choosing wisely the t_{go}, it is possible to balance between computational effort and guidance precision.

The control accelerations computed by the modified ZEM-ZEV guidance result close to the one obtained for the ideal case. Using equations (2.43) and (2.46), the accelerations for the open-loop maneuvers can be computed: $\gamma_x = 2.38 \times 10^{-4}\ m/s^2$ for the Hohmann transfer, while for the closing phase $\gamma_{z_{S_{1-2}}} = 2.04 \times 10^{-5} m/s^2$, $\gamma_{z_{S_{2-3}}} = 1.53 \times 10^{-5} m/s^2$, $\gamma_{z_{S_{3-4}}} = 1.02 \times 10^{-5} m/s^2$, $\gamma_{z_{S_{4-5}}} = 3.58 \times 10^{-6} m/s^2$. If these values are compared with the one obtained from the simulations, it can be observed that they are quite similar. This behavior can be shown in Fig. 4.6, where the guidance accelerations are shown.

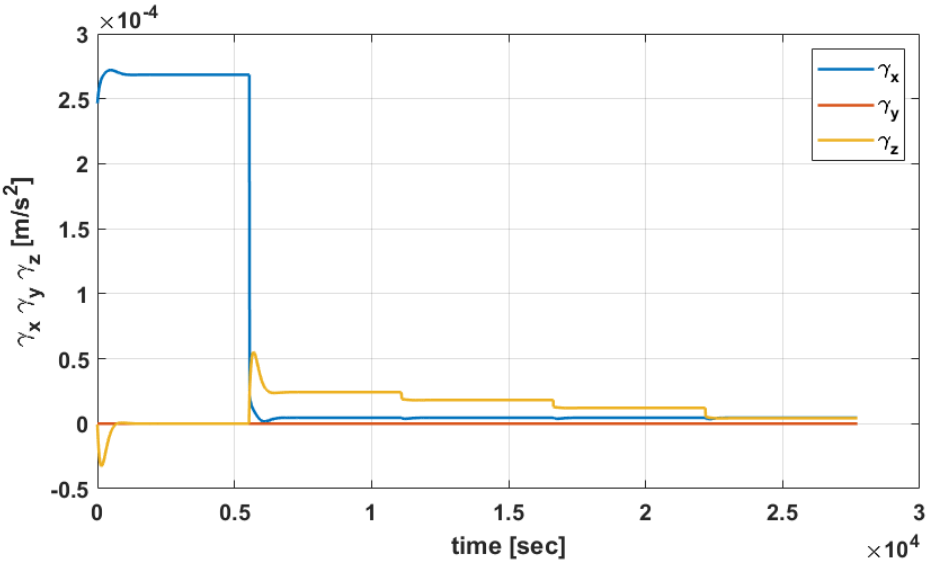

Figure 4.6: ZEM-ZEV accelerations.

It can be noticed that at the start of each trajectory there is an overshooting, which is clearly visible for the maneuvers with higher accelerations required. This error on the fired thrust is corrected along the path and it is related to the t_{go}. In fact, reducing the t_{go}, the overshoot on the acceleration signal is lowered and the guidance is able to compute a better value for the unit thrust from the start.

In Fig. 4.7 and 4.8 the positions and velocities through all the maneuver are shown as a function of time. It can be noticed that the position and velocities are null along the H-bar. This is due to the fact that the maneuver is completely

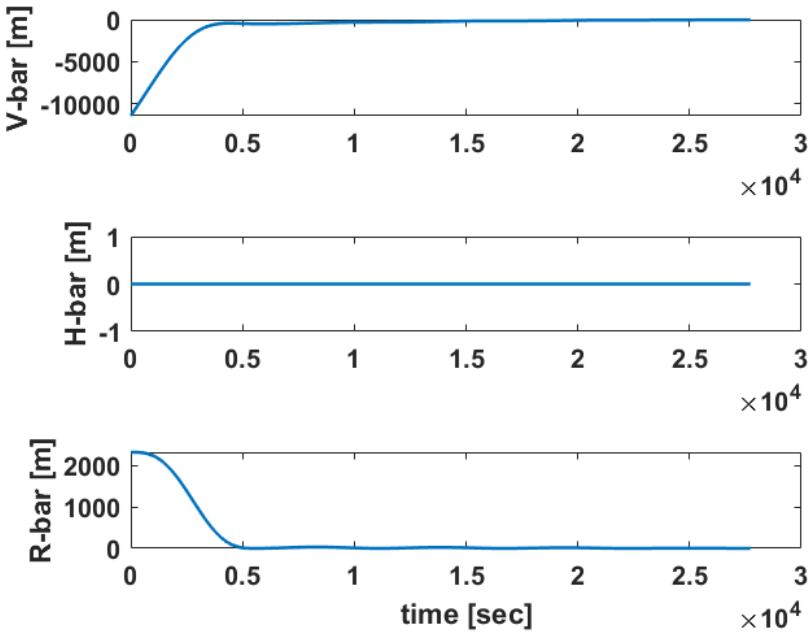

Figure 4.7: Chaser positions along the orbital frame axes.

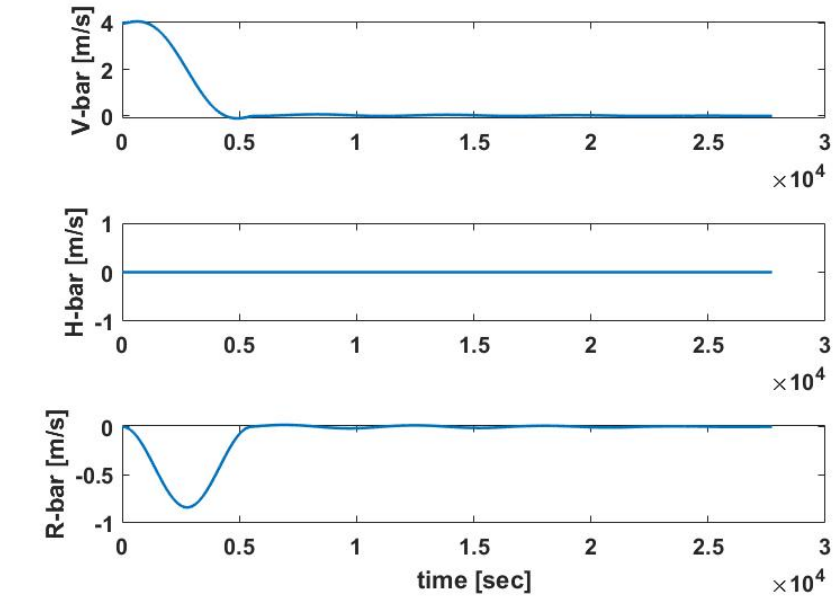

Figure 4.8: Chaser velocities along the orbital frame axes.

executed in the plane V-R of the orbital frame. In fact, in the simulation the position and velocities are null both at the start and at the end of the maneuver along the H-bar, so the control acceleration stays zero. It can be noticed that during the homing phase, which is the first maneuver executed, the velocity is different from zero along the V-bar. This is the drifting velocity of the chaser respect to the target. When the maneuver starts, the velocity grows at first, but then it begins to decrease because of the orbit rising that slows the spacecraft. Instead the velocity along the R-bar, which was initially zero, grows in magnitude until it reaches a pick and then tends to zero again while moving toward the target orbit. The closing phase is executed with radial boosts, so the chaser starts moving along a semicircular orbit toward the target. The velocity profile along the V-bar sees an increase in the first half and then it decreases until it reaches zero relative velocity at the next station-keeping point.

ΔVs maneuver

The ΔVs are now computed applying the equations (2.44) and (2.47) to all the parts of the open-loop maneuver when no disturbances are acting on the spacecraft

Table 4.2: ΔVs, ideal case.

	From S_0 To S_1	From S_1 To S_2	From S_2 To S_3	From S_3 To S_4	From S_4 To S_5	From S_5 To S_6
ΔV	1.317 m/s	0.113 m/s	0.0850 m/s	0.0567 m/s	0.0198 m/s	0.0153 m/s

Summing all the contributions the total cost of the ideal maneuver is obtained, $\Delta Vs = 1.5921 m/s$. The Modified ZEM-ZEV shows to be very efficient in terms of fuel consumption, in fact a $\Delta Vs = 1.6338 m/s$ can be found if the external disturbances are applied and a t_{go} of 300 sec is fixed. It is interesting to notice how the cost also depends on the choice of t_{go}. Higher values of t_{go} mean a superior cost for the maneuver. As it was shown in Fig. 4.6, if the t_{go} grows, the accelerations tend also to increase and to get farther from the ideal value. As a result the cost of the maneuver increase. If instead the t_{go} is reduced, the chaser is forced to follow the desired trajectory with higher accuracy and the accelerations get closer to the ideal one. In this way the cost is reduced and the ΔV tends to the open-loop value.

4.2.2 Short-range Mission

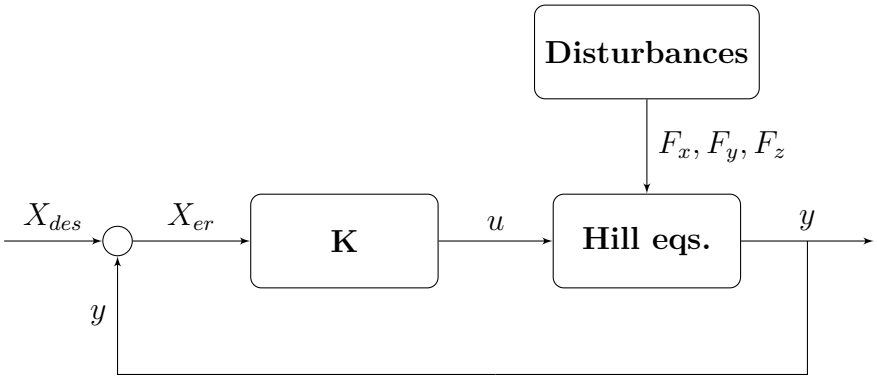

Figure 4.9: LQR, position control block diagram.

This maneuver was developed to describe the proximity operations between the two CubeSats. The Hill equations are still the plant of the system and they describe the relative motion of the chaser. In this case, differently from the long-range maneuver, an LQR controller is developed to make the chaser reaches the final state. The block K represents the gain matrix computed by the LQR theory and it receives as input the state error. As seen in the last chapter, the state error is obtained as a difference between the actual state, y, of the chaser and the one which has to be achieved, X_{des}. Eventual disturbances acting on the chaser are summed to the control action, u, and are the input to the plant block.

The chaser starts its trajectory at the first aim station-keeping point, S_1, 300 m behind the target and 50 m below it. After a continuous V-bar thrust maneuver the chaser reaches the second station keeping point, S_2, on the target orbit. Here a closing phase is started where a series of radial boost maneuvers are implemented until the CubeSat reaches 3 m behind the target in S_5. After the first part of the approach, an escape maneuver is tested. In this scenario it is considered the eventuality of a failure occurring and causing a safety hazard when the chaser is in the proximity of the target. To avoid a possible collision, a maneuver is implemented where the chaser starts moving away from the target reaching a final position of 50 m behind it, or 30 m as an alternative. With these escape trajectories then it can be evaluated the ability of the chaser to abort a docking maneuver in case of collision risk.

Here below in Table 4.3 all the station keeping points are reported. In Fig. 4.11 and 4.12 the complete maneuver is shown from the start to the end (homing, closing

and collision avoidance) with the two different collision avoidance maneuvers.

Table 4.3: Orbit frame Station Keeping points.

SK	Definition	Position [m]
S_1	V-bar maneuver starting position	[-300,0,50]
S_2	V-bar maneuver final position/1° R-bar maneuver initial position	[-64,0,0]
S_3	1° R-bar maneuver final position/2° R-bar maneuver initial position	[-50,0,0]
S_4	2° R-bar maneuver final position/3° R-bar maneuver initial position	[-15,0,0]
S_5	3° R-bar maneuver final position/Escaping trajectory initial position	[-3,0,0]
S_6	Escaping trajectory final position	[-50/30,0,0]

Figure 4.10: Short-range maneuver second case

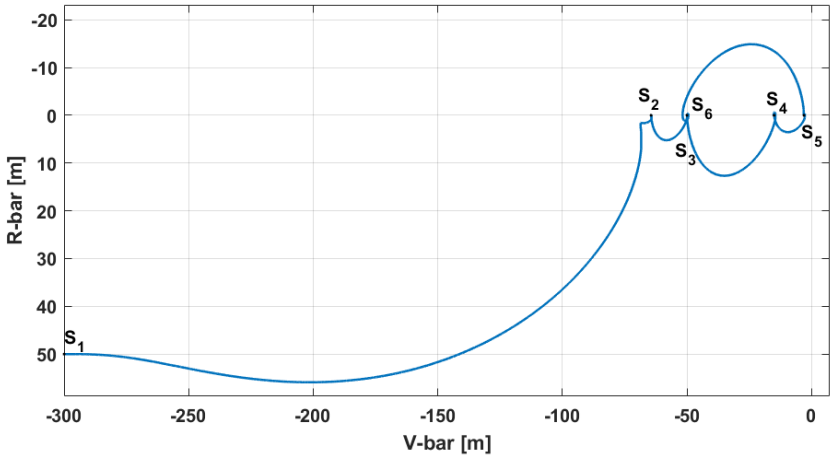

Figure 4.11: Short-range maneuver first case.

For each part of the maneuver the weighting matrices, Q and R, are tuned and the gain matrix is computed off-line. The main advantage of the controller is the simplicity and the low computational effort, although it does not seem to be very precise in following the desired trajectory. In the first maneuver, for example, it can be clearly observed how the chaser tends to lower its altitude before starting to rise toward the target orbit. In fact, if the shape of this path is compared with the ideal one shown in Fig. 2.10 a visible error can be observed.

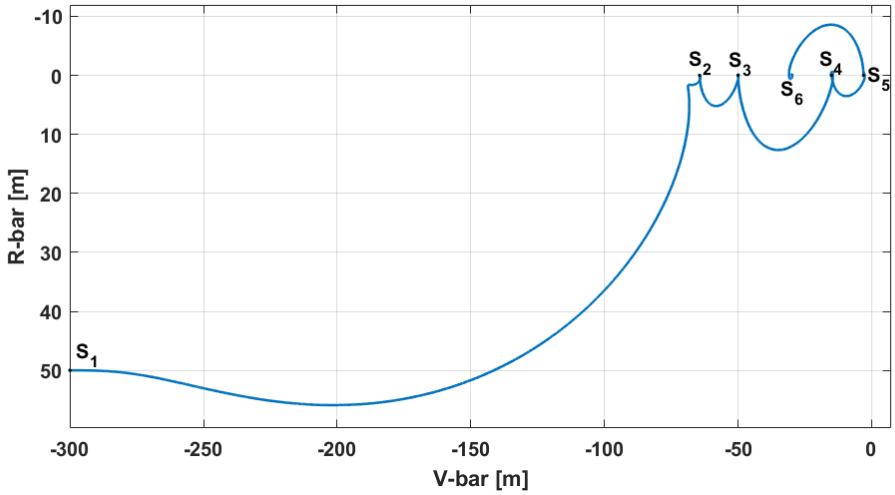

Figure 4.12: Short-range maneuver second case.

It is also interesting to evaluate the control accelerations generated by the controller. It can be seen in Fig. 4.13 how the LQR law tries to follow the desired trajectory firing in the same direction as for the ideal case: during the rising orbit maneuver the main acceleration is the one along the V-bar, while during the closing the thrust is directed along the R-bar.

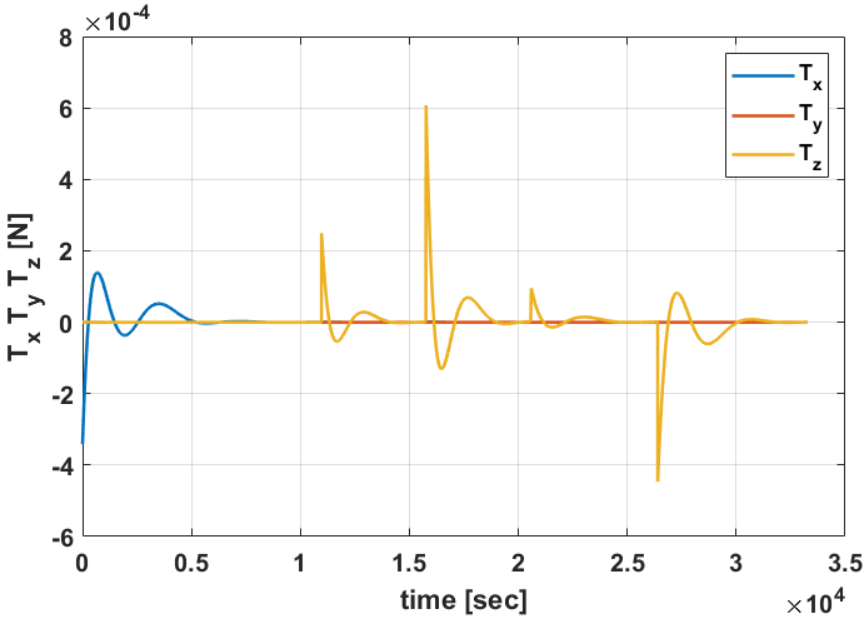

Figure 4.13: LQR control thrust.

Differently from what it was observed with the modified ZEM-ZEV, here the controller tends to generate an high acceleration peak to start the maneuver, followed by lower commands to adjust position and velocity while moving toward the final state. The consequence is that in media the accelerations are higher and the fuel consumption grows.

In Fig. 4.14 and 4.15 the positions and velocities are shown as a function of time. The motion of the chaser stays on the Vbar-Rbar plane, in fact position and velocities along the H-bar are very small. As a consequence of the accelerations applied from the controller, it can be observed that during the rising orbit maneuver the velocities along the V-bar and R-bar tend to increase. In fact the controller initially applies a negative acceleration along the V-bar in order to slow down the chaser which is moving with an initial drifting velocity. So the chaser moves to a slightly lower orbit, as can be observed in the positions plot, and this causes an increase in velocity both along the V- and R-bar. After few seconds in fact the acceleration along the V-bar becomes positive and the spacecraft starts to rise his position toward the target orbit. The V-bar velocity starts then to decrease while the R-bar component turns negative. The behavior during the closing phase is instead very similar to what observed in the ideal case.

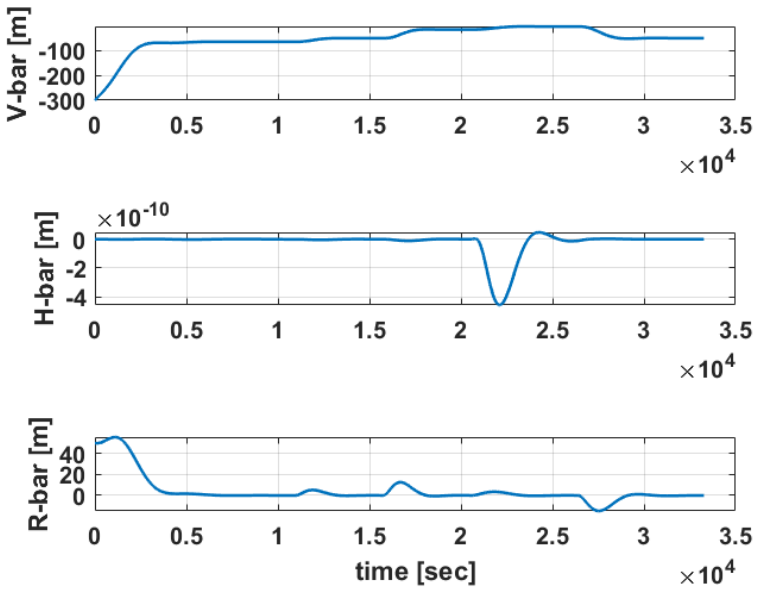

Figure 4.14: LQR positions along local orbital frame axes.

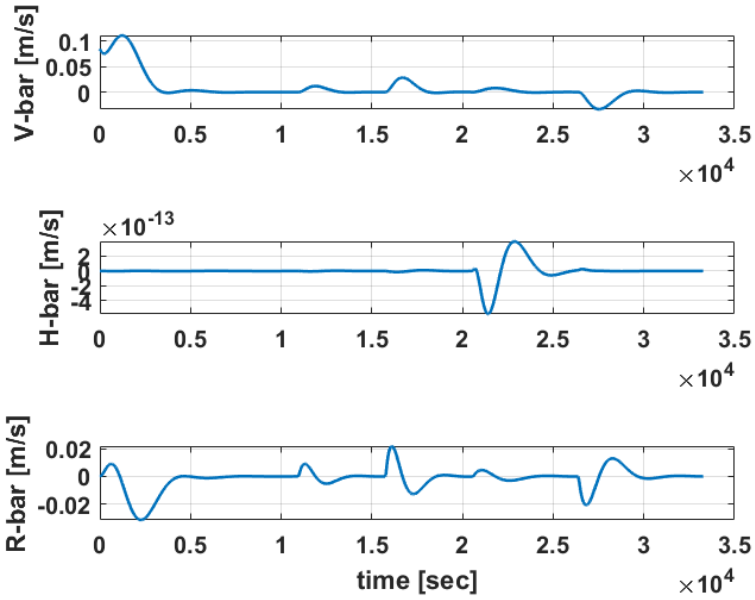

Figure 4.15: LQR velocities along local orbital frame axes.

ΔVs maneuver

So based on the maneuver defined above and applying the equations (2.44) and (2.47), the ΔVs are computed for each part of the maneuver and then the total cost is obtained. The results are for the ideal case with no disturbances considered.

Table 4.4: ΔVs, ideal case.

	From S_1 To S_2	From S_2 To S_3	From S_3 To S_4	From S_4 To S_5	From S_5 To S_6 (First scenario)	From S_5 To S_6 (Second scenario)
ΔV	0.0283 m/s	0.0079 m/s	0.0198 m/s	0.0068 m/s	0.0266 m/s	0.0153 m/s

In the table above the partial ΔVs for each part of the maneuver are computed, so it is now possible to sum them up and show the total ΔVs for the first and second scenarios, Table 4.5.

In terms of ΔVs it can be noticed from the simulations that the LQR control does not perform in a very efficient way in terms of fuel consumption, if the results

Table 4.5: ΔV_{tot} for first and second scenario, ideal case.

	First scenario	Second scenario
ΔV_{tot}	0.0894 m/s	0.0781 m/s

are compared with the values above. In fact, trying to balance the weighting matrices to obtain a good compromise between precision and cost, it was not possible to obtain ΔVs lower than three times the ideal values in the tables.

4.2.3 Attitude control

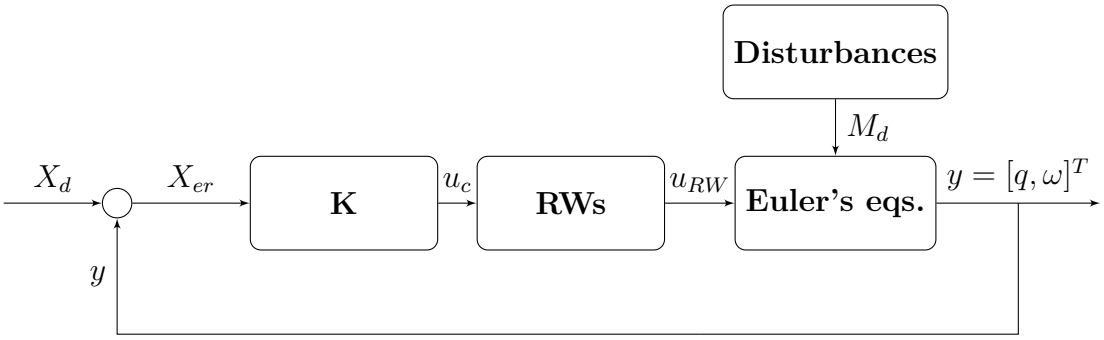

Figure 4.16: LQR, attitude control block diagram.

For the short-range maneuver an attitude control is also implemented. The algorithm developed is again an LQR control. In this case though, the dynamic equations are non-linear, so to compute the gain matrix it was first necessary to linearise the Euler's equations. The input to the controller is the state vector which is given by the difference between the actual and the desired state. A control torque is produced by the controller and it is also the input of the reaction wheels block which is designed as a simple low-pass filter to consider the limitations in the acceptable bandwidth. The output of the plant is the orientation and angular velocity of the chaser in the body reference frame, while the input is the torque from the reaction wheels and the external disturbances.

To test the behavior of the attitude control, an initial rotation of 20 degrees is given to the chaser respect to the desired orientation, in which the spacecraft $\hat{x}_B$ axis in body frame should be aligned to the orbital frame $\hat{V}$-bar. Quaternions and quaternion error are shown in Fig. 4.17 and 4.18. The starting orientation is expressed as $q_{in} = [0.9848, 0, -0.9848, 0]^T$ and the one to reach is $q_f = [1, 0, 0, 0]^T$.

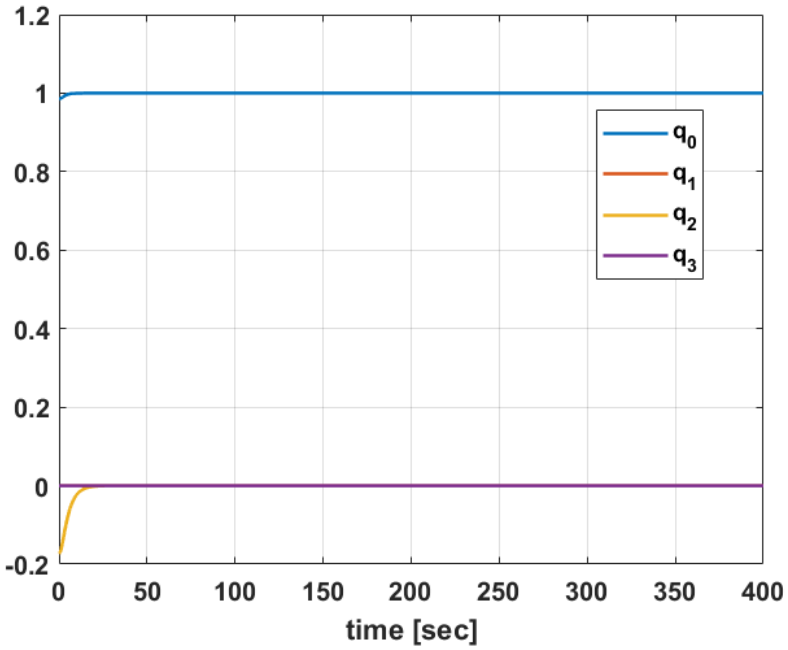

Figure 4.17: Quaternions.

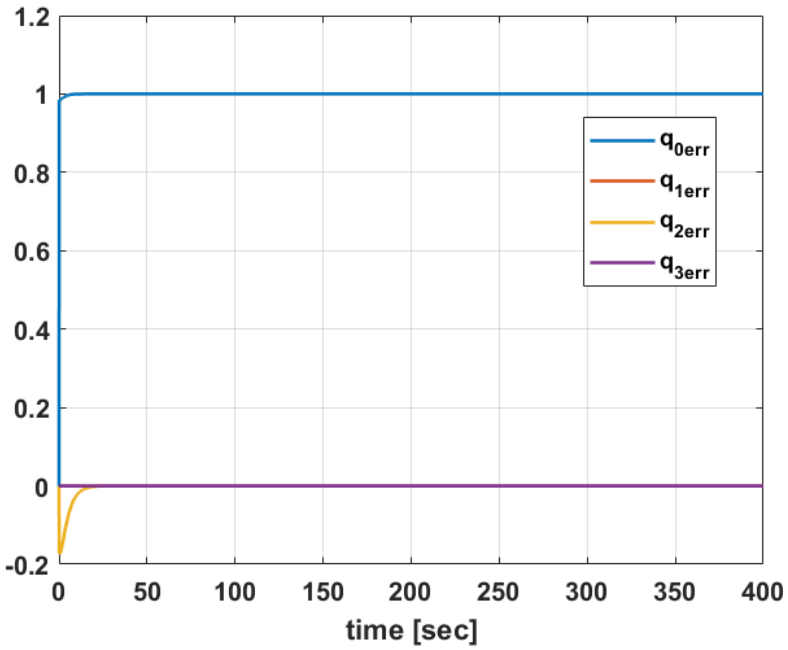

Figure 4.18: Quaternion errors.

In the figures below, the torques from the reaction wheels, Fig. 4.19, and the angular velocities, Fig. 4.20, are shown. As can be seen from the quaternions, the spacecraft starts with a counter-clock wise orientation of -20 degree along the $\hat{y}_B$ axis, so the reaction wheels act to bring the chaser to the desired orientation. The more significant torque component is then M_y, because along that axis the reaction wheel needs to stabilize the spacecraft against the external torques and, at the same time, actively change its orientation. A typical shape can be observed in the torque, M_y: an initial peak to start the chaser rotation, followed by an overshoot in the opposite direction to reduce the angular velocity and stop the spacecraft once the final state is reached. Along the other axes, instead, the control torques are used only to counteract the external disturbance effects, so the values registered are very low. This can be clearly observed looking at the angular velocities, ω_x and ω_z. In fact they are very low which means that only a small variation of angular momentum is needed along $\hat{x}_B$ and $\hat{z}_B$ axes.

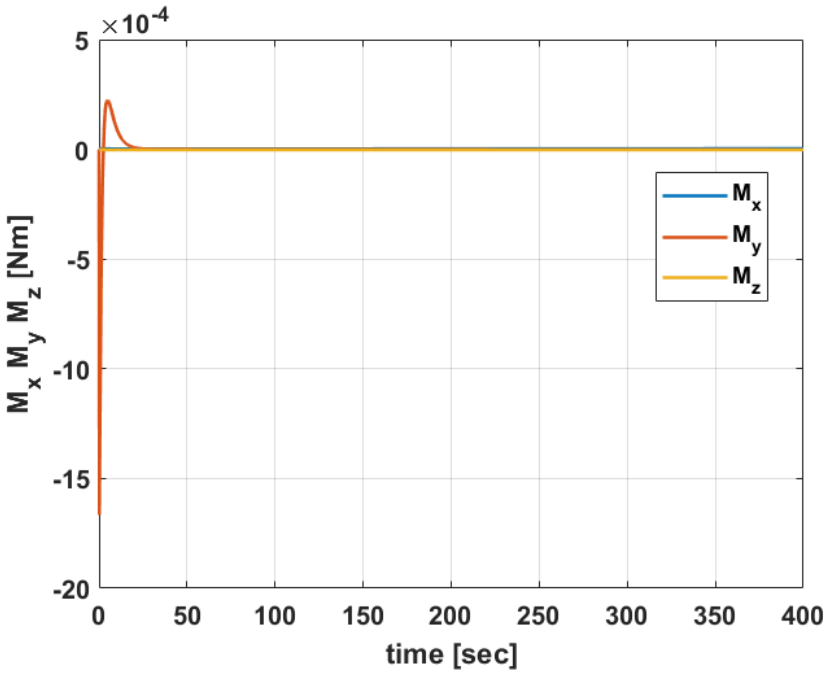

Figure 4.19: Torques from the reaction wheels.

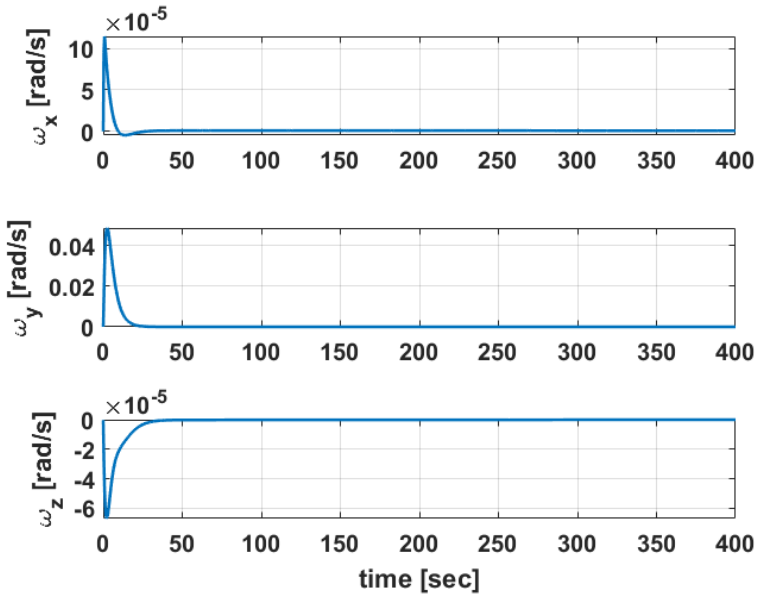

Figure 4.20: Angular velocity along the body axes.

4.2.4 Attitude and Orbit Control System

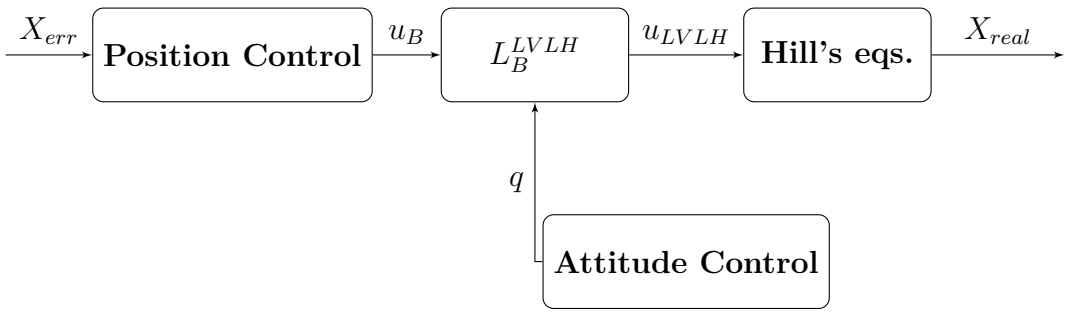

Figure 4.21: Attitude and position control block diagram.

In order to consider the spacecraft as a 3D body during the rendezvous maneuver, the attitude control block is added to the scheme. The position control provides the thrust needed in the body reference frame, so, knowing the spacecraft orientation, it is possible to find the components of the thrust vector in the orbit frame. These components are then the input to the Hill's equations which give the position and velocity of the chaser. A transformation matrix is defined, L_B^{LVLH}. The orientation of the spacecraft is influenced by the environmental disturbances and the reaction wheels act to minimize the state error and keep the chaser along

the desired orientation.

As it can be seen in Fig. 4.22, with the position and attitude algorithms together, it is still possible to obtain for the maneuver a shape very similar to the one achieved before for the position control only. The most visible difference in the trajectory is during the homing phase, where the chaser tends to reach a lower minimum before starting to raise. This is mainly an effect of the initial error in the spacecraft orientation. In fact, as shown in Fig. 4.23, the initial acceleration along the V-bar is doubled respect to the case without attitude control, and this is due to the fact that the position control has to overcome the initial error in orientation which reduces the effective thrust component. Once the chaser reaches the final orientation, the effect of the external disturbances is not so relevant and the control thrust required for the maneuver results very close to the case without attitude control. This is clear from Fig. 4.13.

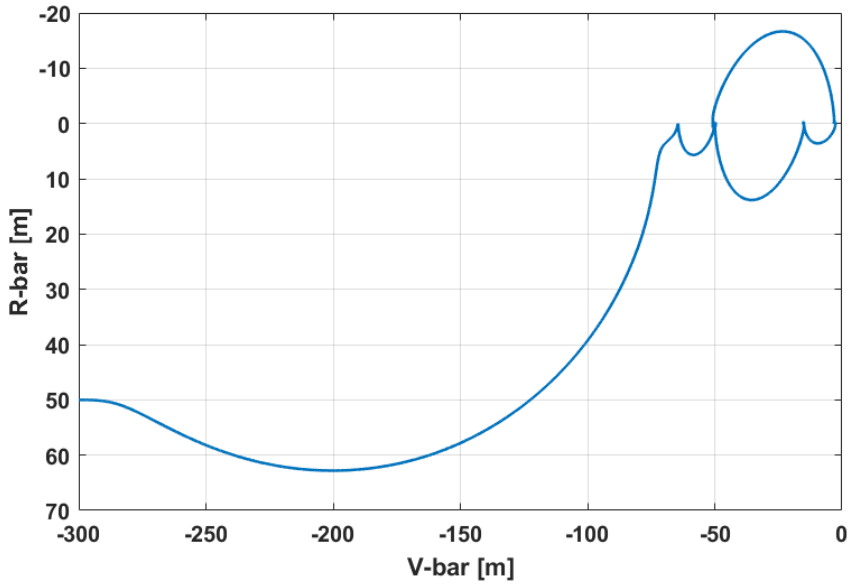

Figure 4.22: AOCS maneuver.

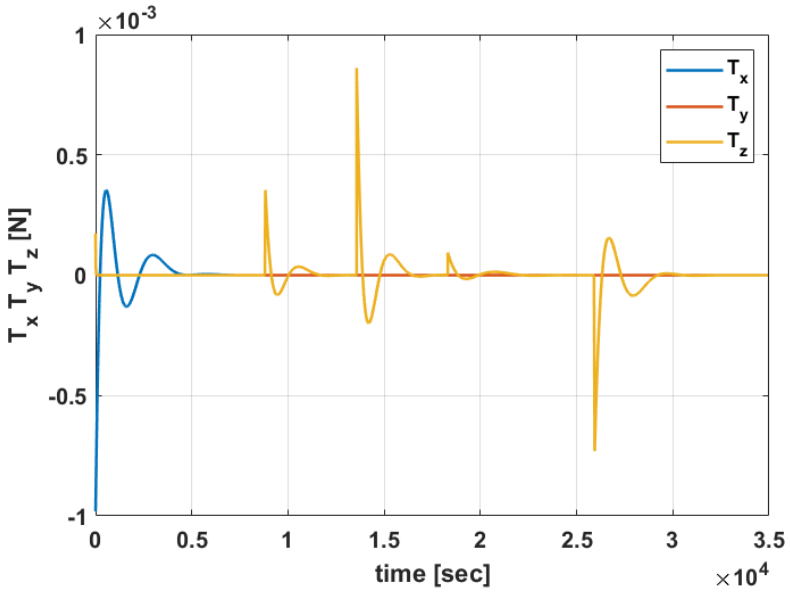

Figure 4.23: AOCS thrust.

In Fig. 4.22 and 4.25 the position and velocities as a function of time are shown. The shape of the maneuver here depicted is the same described before. It is interesting though, to notice that the oscillations in position of the chaser along the H-bar are bigger than the one observed for the position control alone. This is a consequence of the error in orientation caused by the external torques, which also generates a component of thrust out of the maneuver plane.

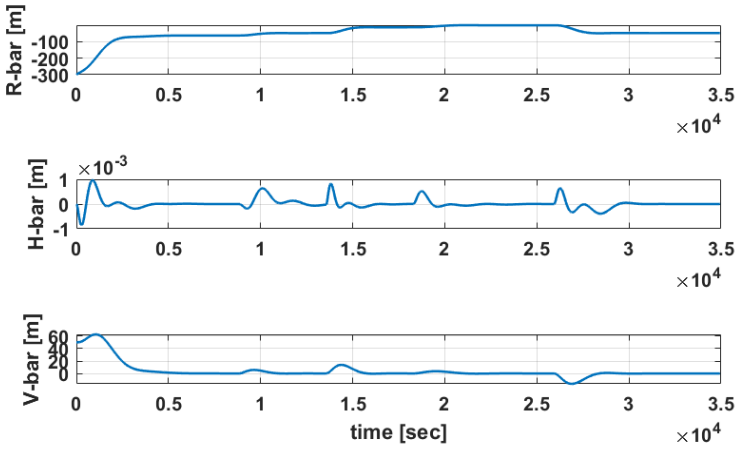

Figure 4.24: AOCS positions as function of time along the orbital frame axes.

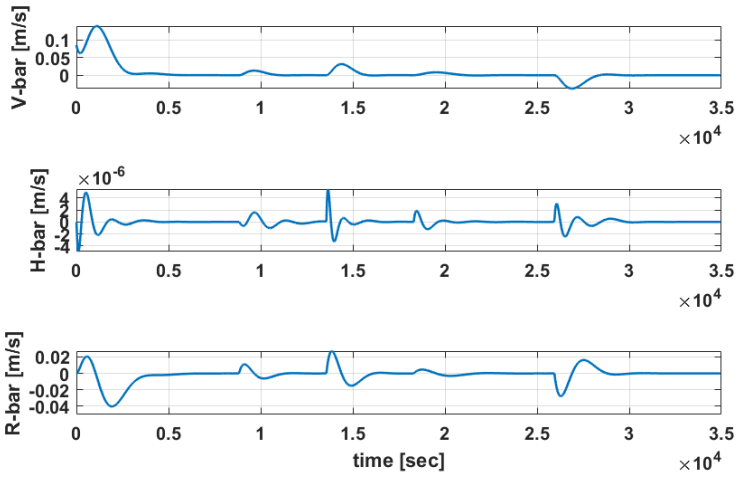

Figure 4.25: AOCS velocities as function of time along the orbital frame axes.

In Fig. 4.26, the external disturbances are shown as a function of time. As it can be seen, in this research the aerodynamic torque, the gravity gradient and the magnetic torque are considered. These are the most relevant disturbances for a spacecraft on a LEO orbit.

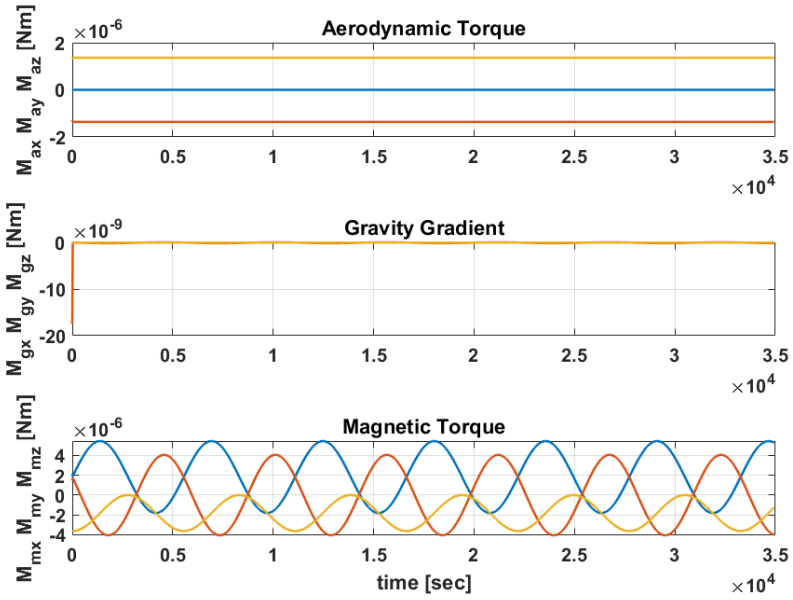

Figure 4.26: Disturbances: Aerodynamic Torque, Gravity Gradient, Magnetic Torque.

Chapter 5

Closing and Future Work

In this research, the problem of rendezvous between two CubeSats has been studied. The aim is to develop and test the performance of guidance and control algorithms for different approach scenarios. The simulations are designed using MATLAB/Simulink.

The first presented case is a long-range maneuver and a modified ZEM-ZEV guidance is applied to control the position and velocity along the trajectory. The obtained results are very promising, in fact the guidance allows the chaser to follow the desired maneuver with high precision, the control accelerations tend to the ideal values and the fuel consumption is optimized. On the other side, the performance of the ZEM-ZEV strongly depends on the time-to-go. So to obtain high accuracy and low impulse of velocity, it is necessary to choose low values of time-to-go with an inevitable increase in the computational effort. Then a balance has to be found based on the processing capabilities of the on board computer.

The other developed case is an LQR controller for a short-range maneuver. Both a position and an attitude control are designed for this scenario. The considered approach is to compute the weighting matrices and the gains for each trajectory off-line, during the variables initialization. The main advantages of this approach are the simplicity in tuning and the low computational effort, considering that all the gains are computed before the simulation starts. The results of the position control show that the chaser is able to follow the desired trajectory but with a reduced precision if compared to the ZEM-ZEV. Higher accuracy can be obtained only accepting an increase in fuel consumption, which is in general avoided for CubeSat missions. For the attitude control, instead, three reaction wheels are implemented and tested to maintain the desired orientation acting against the external disturbances. From the simulations it can be observed that the disturbances are damped quite fast and the state error tends to zero.

For the future it could be interesting to design the final approach for both the maneuvers and test if the guidance and controller are able to guarantee a sufficient

level of accuracy to accomplish the docking between the CubeSats. A path planning algorithm could be studied to avoid collisions during the last phase. The modified ZEM-ZEV as studied in this research presents some significant problems that have to be resolved. As explained in [16] and [30], the algorithm is not robust to uncertainties and, it also lacks in flexibility and capacity to adapt in real time. Other researches have considered these problems and improved the ZEM-ZEV combining it with a sliding mode control [31] or with a model predictive approach [32] or with machine learning [30]. All of them are applied to the landing problem, so it could be interesting to study these algorithms for the rendezvous maneuver. For the short-range maneuver a possible improvement could be to redesign the LQR controller online, with different gain matrices. As shown in [17], this solution seems to produce results with high accuracy and, at the same time, with a sub-optimal fuel efficiency.

Bibliography

[1] M. E. Polites. *An Assessment of the Technology of Automated Rendezvous and Capture in Space*. An Assessment of the Technology of Automated Rendezvous and Capture in Space, 1998 (cit. on p. 1).

[2] Bradley W. Carroll. «The delicate dance of orbital rendezvous». In: 87 (Aug. 2019), pp. 627–637 (cit. on pp. 1, 2).

[3] Wigbert Fehse. *Automated Rendezvous and Docking of Spacecraft*. Cambridge University Press: Cambridge University Press, 2003 (cit. on pp. 1–4, 11, 14, 21–25).

[4] Martine Ganet Isabelle Quinquis Jerome Bourdon Patrick Delpy. «ATV GNC during Rendezvous with ISS». In: (Jan. 2002) (cit. on pp. 1–4).

[5] Hirohiko Uematsu Satoshi Ueda Toru Kasai. «HTV Rendezvous Technique And GN&C Design Evaluation Based on 1st Flight On-orbit Operation Result». In: (Aug. 2010) (cit. on pp. 1–3).

[6] R. Murtazin N. Sevastiyanov N. Chudinov. «Fast rendezvous profile evolution: FromISSto lunar station». In: (Apr. 2020) (cit. on p. 2).

[7] P. Miotto L. Breger I. Mitchell B. Keller and B. Richikot. «Designing and validating proximity operations rendezvous and approach trajectories for the cygnus mission». In: (Apr. 2020) (cit. on p. 2).

[8] Camille Sébastien Pirat. *Guidance, Navigation and Control for Autonomous Rendezvous and Docking of Nano-Satellites*. Lausanne: ÉCOLE POLYTECHNIQUE FÉDÉRALE DE LAUSANNE, 2018 (cit. on pp. 4–6, 25, 40, 44).

[9] Elisa Capello Fabrizio Dabbene Giorgio Guglieri Elisabetta Punta. «Flyable Guidance and Control Algorithms for Orbital Rendezvous Maneuver». In: 11 (Jan. 2018) (cit. on pp. 5, 6).

[10] Bong Wie Matt Hawkins Yanning Guo. «Spacecraft Guidance Algorithms for Asteroid Intercept and Rendezvous Missions». In: J. of Aeronautical & Space Sci (June 2012) (cit. on pp. 5, 6).

[11] Pin-Jar Yuan Shih-Che Hsu. «Rendezvous Guidance with Proportional Navigation». In: 17 (Dec. 1993) (cit. on p. 5).

[12] B. Ebrahimi M. Bahrami. «Optimal Sliding-Mode Guidance Law for Fixed Interval Propulsive Maneuvers». In: (June 2008) (cit. on p. 5).

[13] Yao Zhang Yanning Guo Guangfu Ma Tianyi Zeng. «Collision avoidance ZEM/ZEV optimal feedback guidance for powered descent phase of landing on Mars». In: Elsevier Ltd (Dec. 2016) (cit. on p. 6).

[14] Roberto Furfaro Brian Gaudet. «ZEM/ZEV Guidance Approach for Asteroid Touch-and-Go Sample Collection Maneuvers». In: Space Systems Engineering Laboratory (SSEL) (Jan. 2013) (cit. on p. 6).

[15] Giorgio Guglieri Matteo Dentis Elisa Capello. «A Novel Concept for Guidance and Control of Spacecraft Orbital Maneuvers». In: International Journal of Aerospace Engineering (Oct. 2016) (cit. on pp. 6, 33).

[16] Matteo Dentis. *Development of Innovative GNC Algorithms for Aerospace Applications*. Politecnico di Torino, 2018 (cit. on pp. 6, 11, 64).

[17] M. Romano R. Bevilacqua T. Lehmann. «Development and experimentation of LQR/APF guidance and control for autonomous proximity maneuvers of multiple spacecraft». In: Elsevier Ltd (Aug. 2010) (cit. on pp. 7, 38, 64).

[18] Yaguang Yang. «Analytic LQR Design for Spacecraft Control System Based on Quaternion Model». In: Journal of Aerospace Engineering (July 2012) (cit. on p. 7).

[19] David A. Vallado. *Fundamentals of Astrodynamics and Applications*. McGraw-Hill companies (cit. on p. 10).

[20] Giulio Avanzini. *Spacecraft Attitude Dynamics and Control*. Politecnico di Torino, 2008 - 09 (cit. on p. 13).

[21] Brett Newman Mohamed Okasha. «Relative Motion Guidance, Navigation and Control for Autonomous Orbital Rendezvous». In: J. Aerosp. Technol. Manag (Sept. 2014) (cit. on p. 13).

[22] Nirvana. *Rotation Matrix to Quaternion(proper Orientation)*. URL: `https://math.stackexchange.com/q/923293` (cit. on p. 17).

[23] Drives & Control. «DC motors stabilise Scotland's first satellite». In: () (cit. on p. 21).

[24] Peter Reid. «Schematic illustration of Earth's magnetic field». Edinburgh, UK: The University of Edinburgh (cit. on p. 27).

[25] Mark L. Psiaki. «Magnetic Torquer Attitude Control via Asymptotic Periodic Linear Quadratic Regulation». In: Journal of Guidance, Control and Dynamics (Mar. 2001) (cit. on p. 28).

[26] M. Farissi S. Carletta A. Nascetti P. Teofilatto. «Implementation and Hardware-In-The-Loop Simulation of a Magnetic Detumbling and Pointing Control Based on Three-Axis Magnetometer Data». In: (Dec. 2019) (cit. on p. 28).

[27] Alex Zaliznyak David Stern. «Gravity Gradient». In: CC-BY-SA 3.0. () (cit. on p. 28).

[28] Bong Wie Jaemyung Ahn Yanning Guo. «Precision ZEM/ZEV Feedback Guidance Algorithm Utilizing Vinti'S Analytic Solution of Perturbed Kepler Problem». In: AAS () (cit. on p. 31).

[29] Matlab/Simulink. *Discretizing and Resampling Models*. Vol. Online Documentation. URL: `https://uk.mathworks.com/help/control/ug/discretizing-and-resampling-models.html` (cit. on p. 41).

[30] Roberto Furfaro Andrea Scorsoglio Richard Linares Mauro Massari. «Adaptive Generalized ZEM-ZEV Feedback Guidance for Planetary Landing via a Deep Reinforcement Learning Approach». In: Acta Astronautica (Mar. 2020) (cit. on p. 64).

[31] Roberto Furfaro Daniel R. Wibben. «Optimal sliding guidance algorithm for Mars powered descent phase». In: Advances in Space Research (Dec. 2015) (cit. on p. 64).

[32] Hyochoong Bang Youeyun Jung. «Mars precision landing guidance based on model predictive control approach». In: J Aerospace Engineering (Aug. 2015) (cit. on p. 64).